Ferroelectric-semiconductor heterostructures for opto-electronic and neuromorphic applications

written by

Laura Seufert

Master Thesis in Physics
presented to the Faculty for Physics, Mathematics
and Computer Science (FB 08)
at Johannes Gutenberg University Mainz
1st September 2020

first supervisor: Prof. Dr. Thomas Palberg
second supervisor: Dr. Kamal Asadi

Ich versichere, dass ich die Arbeit selbstständig verfasst und keine anderen als die angegebenen Quellen und Hilfsmittel benutzt sowie Zitate kenntlich gemacht habe.

Mainz, 1st September 2020

Laura Seufert

Institute for Physics, Johannes Gutenberg-Universität
Staudingerweg 7
55099 Mainz
lseufert@students.uni-mainz.de

Max Planck Institute for Polymer Research
Ackermannweg 10
55128 Mainz
seufertl@mpip-mainz.mpg.de

Contents

1. Introduction **2**

2. Theoretical background **5**
2.1. The ferroelectric polymer P(VDF-TrFE) and ferroelectric switching . 5
2.2. Semiconducting polymers 8
2.3. Thermally activated delayed fluorescence 9
2.4. P(VDF-TrFE):PFO memory diode 10
2.5. Breath figures 12
2.6. Polarisation fatigue in P(VDF-TrFE) 13
2.7. Basic neuromorphic terms 14

3. Experimental **17**
3.1. Materials 17
3.2. Device fabrication 18
3.2.1. Fabrication of porous P(VDF-TrFE) thin films 18
3.2.2. Fabrication of memory diodes 19
3.2.3. Fabrication of P(VDF-TrFE):PFO blend film devices 20
3.3. Structural characterisation 20
3.4. Image analysis 21
3.5. Electrical characterisation 21

4. Results and Discussion **24**
4.1. Porous P(VDF-TrFE) thin films with 3-1 connectivity for phase separated heterostructures with improved morphology used in memory diodes 24
4.1.1. First attempts in the search for porous P(VDF-TrFE) thin films 24
4.1.2. Analysis of the porous P(VDF-TrFE) thin films created by increasing heating time 26
4.1.2.1. SEM imaging for analysis of pore density and diameter 27
4.1.2.2. AFM imaging for analysis of pore depth and measurement of film thickness with DEKTAK profilometer . . 28
4.1.3. Porous P(VDF-TrFE) thin films with 3-1 connectivity 30
4.1.4. Filling the porous P(VDF-TrFE) thin films with semiconducting polymer 32
4.1.4.1. PFO as the semiconductor material 32
4.1.4.2. 4CzIPN as the semiconductor material 35

4.2. Multilevel switching of P(VDF-TrFE):PFO blend film devices for use in neuromorphic applications 37
4.2.1. Initial characterisation 37
4.2.2. Application of voltage pulses to address and read multilevel polarisation states of P(VDF-TrFE) 38
4.2.2.1. Measurement with the Keithley 4200-SCS 38
4.2.2.2. Measurement with high resolution oscilloscope and preamplifier 39
4.2.3. Switching of the polarisation state with variation of amplitude and width of the write pulse 42
4.2.4. Stability of the multilevel polarisation states – retention time and fatigue issues 45
4.2.5. Switching of the polarisation state with increasing number of repetitions of the write pulse 49
4.2.6. Application of pre-spike and post-spike pulses to emulate synaptic behaviour 52
4.2.7. Addressing and read-out of individual P(VDF-TrFE):PFO blend film devices in a 2x2 array 53
4.2.8. Observations for addressing the polarisation states in the P(VDF-TrFE):PFO blend device with voltage pulses 57

5. Conclusion **60**

A. Bibliography **62**

B. Appendix **68**
B.1. Matlab code used for statistical analysis of four SEM images per sample 68
B.2. Additional data and images on porous P(VDF-TrFE) films 72
B.3. Additional data on samples filled with 4CzIPN 78
B.4. Additional data on film thickness in the array 79

C. Acknowledgements **80**

1. Introduction

In the search for non-volatile resistance switching for applications such as information storage, flexible electronics and neuromorphic devices various concepts have been examined. Ferroelectric polymers and organic semiconductors have come of interest, because they can be processed from solution through coating or printing methods and are therefore suitable for low-cost and large area manufacturing [1]. For memory applications the material needs to provide electric-field controlled resistance switching between two (or more) distinct and stable states.
Ferroelectric polymers are suitable candidates for the bistable resistance switching [2]. The most widely investigated organic ferroelectric is the random copolymer of vinylidene fluoride and trifluoroethylene (P(VDF-TrFE)). Thin film capacitors with P(VDF-TrFE) as dielectric exhibit stable polarization states and that can be used as non-volatile memories [3, 4]. However, the read-out of the information stored in such a capacitor is destructive. The external field applied for the read-out can alter the polarisation state. This is solved by combining P(VDF-TrFE) with a semiconductor material. In these ferroelectric-semiconductor heterostructures P(VDF-TrFE) provides bistable resistance switching and the semicondutor provides the conduction [5].
In order for the conduction through the semicondutor to not be hindered by the insulating P(VDF-TrFE) the heterostructure has to be laterally divided with semiconducting columns embedded in the ferroelectric matrix (compare figure 1.1). Dependent on the orientation of the ferroelectric polarisation the current density through the semiconductor is low (OFF state) or high (ON state). The semiconductor enables non-destructive read-out of the programmed state with voltages lower than the coercive state of the ferroelectric. Diodes using poly(9,9-dioctylfluorene) (PFO) as the semiconducting material with bistability and an ON/OFF ratio approaching 1×10^4 were shown [6].
This work comprises two different projects using P(VDF-TrFE):PFO heterostructure device. Firstly it was focused on making advanced in creating the ideal morphology of the heterostructure. The most common method applied are the blend films, that utilise that the polymers generally do not mix and phase-separate due to low enthalpy of mixing and small entropic gain [7]. The two polymers are dissolved in a common solvent and the thin films are produced with coating techniques. In the resulting film not all the semiconductor domains embedded in P(VDF-TrFE) are continuous through the film (compare figure 1.1 (a)) and therefore cannot transport charges from the bottom to the top electrode. Through selective washing it has been shown that only two thirds of the semiconductor material are in functioning domains [8]. This method also lacks control of the domain size, which is of disadvantage for area scaling.

As can be seen in figure 1.1 (a) the blend film method also results in intermixing of the components at the interface between the domains. Since simulation has shown that the charges transported through the semiconductor domains are very strongly located at the interface, this is of high importance for the device performance [9]. A first MEMOLED of PFO and P(VDF-TrFE) processed with the blend method was demonstrated [10]. The advantage of the heterostructure allows to address the organic light emitting diode actively, through modulation of the polarisation in P(VDF-TrFE), in a passive matrix geometry. The efficiency (ratio of light emission and current output) for the MEMOLED was at least an order of magnitude lower than that of a conventional LED using PFO as the semiconductor.

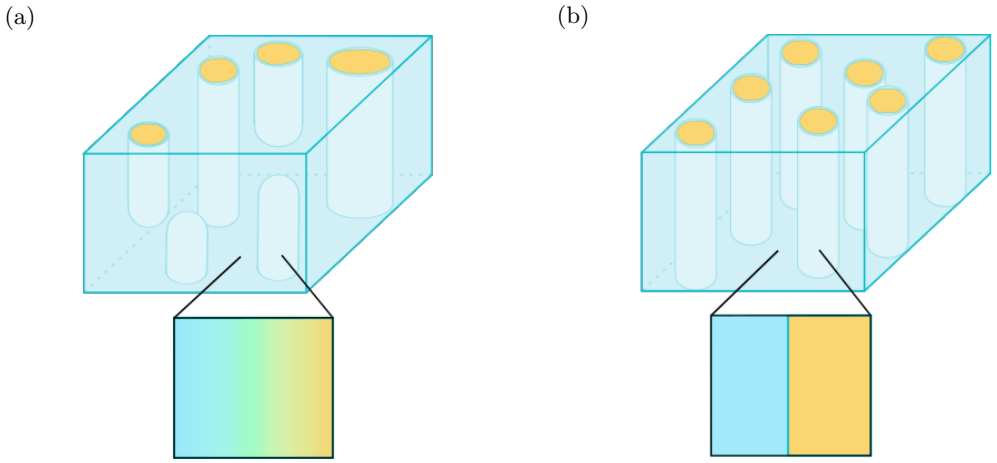

Figure 1.1.: Comparison of phase separated ferroelectric-semiconductor heterostructures created by **(a)** the common blend film method and **(b)** the proposed backfilled pores method.

Another method applied for optimizing the microstructure is patterning. This method uses lithography or micromolding to create a regular array of one component and then fill up voids with the second component [11, 12, 13]. While this allows to determine the domain size and distribution, large-scale production could be complicated by the need for top-down patterning. Additionally the filling of the voids with the semiconductor created a continuous film of that material on top of the heterostructure, which could lead to crosstalk and was shown to negatively impact the memory performance [14]. This work shows a new method for fabrication of P(VDF-TrFE):PFO lateral heterostructures with all semiconductor domains bicontinuous, sharp interfaces between the materials and the ability to control the domain size (compare figure 1.1 (b)). First porous P(VDF-TrFE) thin films with pores of 3-1 connectivity (see domain structure in 1.1 (b)) were produced by utilising a breath figure method under controlled humid atmosphere and followed by heating. This has not been demonstrated before. Then the created pores were backfilled with the semiconducting material PFO and, making use of the versatility of the porous films, also with the small molecule TADF semiconductor 4CzIPN.

In the second project using P(VDF-TrFE):PFO heterostructures the suitability of these thin films for neuromorphic applications was explored. Typically the memory diode is used in either the fully depolarised or fully polarised state. However, P(VDF-TrFE) can also be partially polarised with good retention time of the intermediate polarisation states, which enables multi-bit memory applications, that allow higher storage density [15, 16, 17]. Therefore the memory diodes are a good candidate for neuromorphic applications [18]. This work demonstrates the gradual resistance switching into several stable states through application of voltage pulses for the P(VDF-TrFE):PFO memory diode for the first time. The control of the polarisation state through adjustment of the voltage pulse width and amplitude is systematically examined. Program and read operations are shown for an array of the diodes, which has not been demonstrated before. Besides the potential of the memory diode for emulating the biological systems in the human brain as an artifical synapse are shown.

2. Theoretical background

2.1. The ferroelectric polymer P(VDF-TrFE) and ferroelectric switching

The ferroelectric polymer polyvinylidene fluoride (PVDF) consists of the CH_2-CF_2 vinylidene monomer, which alternately has a pair of hydrogen and a pair of fluorine atoms bound to the carbon backbone. There are four crystalline phases of PVDF known, including the most stable, non-ferroelectric α phase and the three ferroelectric β, γ and δ phases. Doping PVDF with other polymers like trifluoroethylene (TrFE), in which one hydrogen atom is replaced by a fluorine atom (see figure 2.1), helps to stabilize the copolymer in the ferroelectric β phase [19]. P(VDF-TrFE) is a highly durable, non-toxic and air-stable polymer.

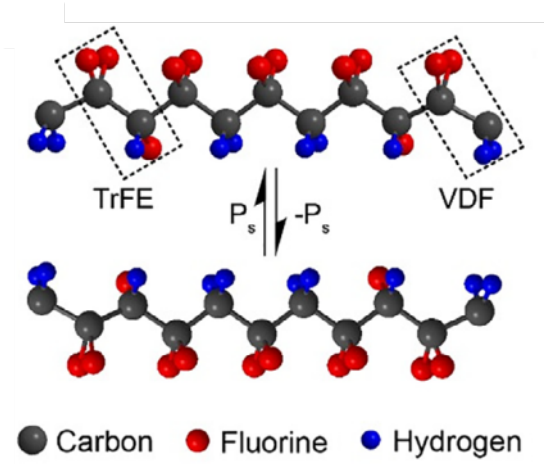

Figure 2.1.: P(VDF-TrFE) in its two fully polarised states with all dipoles oriented parallel to each other (image taken from [19]).

By orientation of the side groups the P(VDF-TrFE) molecule builds up a dipole moment due to the presence of strongly electronegative fluorine atoms, which can be aligned by an externally applied electric field. Two antiparallel orientations of the dipoles are observed, when an electric field is applied. Regions of the sample which contain a uniform dipole orientation are called domains. For P(VDF-TrFE) one observes switching between the two domain states by applying an electric field which favours one of them. The boundary separating two domains is referred to as a domain wall and the domain wall velocity is a parameter, which is used to describe the

switching process (see source [20], also for the following paragraphs).
Under ideal conditions, where no field is applied and we have perfectly oriented polymers, both domain states have the same energy density, but within the wall the structure is distorted. Therefore the domain boundary contains some extra energy, which leads to a passage between the two states.
Changes on a molecular level are accompanied by variation of the macroscopic polarisation vector. The domain state reorientation is determined by measuring the polarisation and referred to as the switching process.
When an electric field is applied to a P(VDF-TrFE) film we expect the growth of domains with structures preferred by the applied field at the expense of domains with other structures. The polarisation variation associated with this phase transition is termed spontaneous polarisation P_s. The magnitude and direction of P_s can be determined by measuring the transported charges by integrating the electric current. For a ferroelectric material mapping of the change in polarisation versus the applied field will lead to the observation of a hysteresis loop. This indicates the stability of either of two states when the applied force is zero and is the basis of applications with non-volatile random access memory.
While the states on the hysteresis loop are transient, there is a possibility of multidomain states existing in static conditions as well. These are often metastable states, which can have a long lifetime. One speaks of a single domains sample, if the total volume of a sample represents just one of the domain states. A real sample will always be multidomain with domains coexisting in it, since defects may prefer the presence of two domains next to each other and metastable domain patterns may remain from dynamic processes. In practice the reorientation is accomplished only in parts of the sample and it results in a multidomain sample. Those samples are not in the ground state of energy, because the domain wall represent perturbations of the structure. The field created by a charged wall therefore increases the energy of the system as a whole and may also suppress ferroelectricity in the neighbouring domains. Thus, there is a limit to the maximum value of surface charge density beyond which the wall cannot exist. Several factors contribute to the orientation of a domain wall: (a) the domain state with the wall of a given orientation should at least correspond to a local energy minimum, (b) electrostatic energy caused by differently oriented P_s vectors and (c) elastic energy due to differently oriented spontaneous strains in neighbouring domains, and (d) energy of the wall itself.
The polarisation switching in a uniformly polarized sample can be described by the Kolmogorov-Avrami-Ishibashi (KAI) model in four steps: (i) nucleation of domains, (ii) longitudinal growth of domains along the direction of the applied electric field, (iii) transverse growth of domains and (iv) coalescence of domains until the polarization in the region is entirely reversed. The starting point will be an “almost single domain” state, which will still contain some metastable or stable “frozen-in” nuclei of opposite dipole orientation as explained above (see figure 2.2 (a)). Upon application of a field directed against the dominant polarisation direction these nuclei will start to grow along the ferroelectric axis. In a separate process new nuclei are formed in many spots of the sample independently (figure 2.2 (b)). The nucleus can only grow,

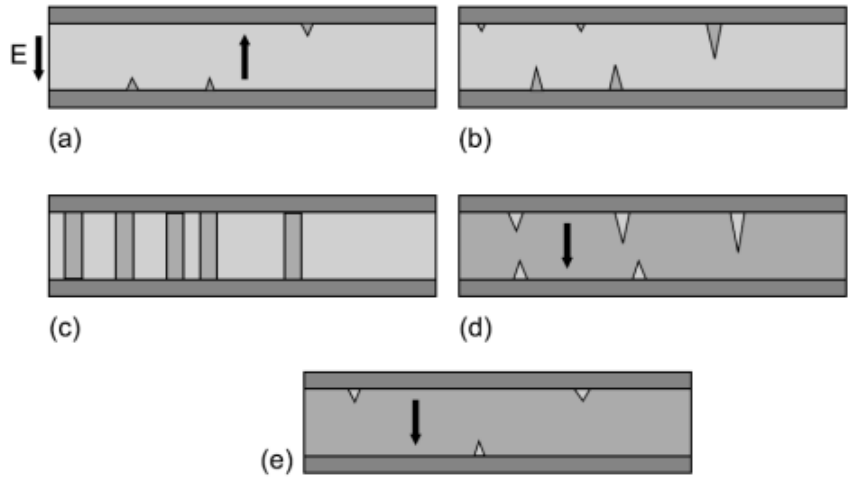

Figure 2.2.: P(VDF-TrFE) thin films with its two fully polarised states shown in light and dark grey (image taken from [20]). (a) Almost uniformly polarised initial state, (b) and (c) longitudinal growth of the domains with dipole orientation in the direction of the applied electric field, (d) transverse growth of domains until the sample is almost uniformly polarised along the direction of the applied electric field (e).

when its energy exceeds a certain critical value. The growth of these supercritical domains reduces the energy of the whole sample. The domain wall velocity exhibits anisotropy, with the domain boundaries growing faster in longitudinal direction than in transverse direction ($v_{long} > v_{trans}$) (this can be observed in figure 2.2 (c)). For thin films the difference is about one order of magnitude [21]. Thus the grown-up nucleus first reaches both electrodes and forms a narrow domain, before phase (iii) of transverse growth is dominant. As the transverse growth continues and the switched domains approach each other, it becomes easier to described the shrinking domains of the original domain state rather than to growing domains of the resulting domain state (figure 2.2 (d)). This is referred to as domain coalescence. Finally the sample is again in an almost homogeneous domain state oriented along the field. Some small metastable domains or frozen-in nuclei of the original polarisation direction will again remain in the sample (see figure 2.2 (e)).
In the measurement of the hysteresis loop a DC voltage is applied to the sample, but it is also possible to switch the sample with voltage pulses. When a pulse is applied the current signal shows a first sharp current peak corresponding to the linear capacitance of the sample, not connected to any domain phenomena. Afterwards a certain backswitching takes place as the system relaxes to a stable state after the previous polarization reversal process. The length of the field pulses determines whether the switching process is fully completed or only partially. If a series of voltage pulses shorter than a critical pulse length are applied, there is no net reversal of P_s. The critical pulse length is dependent on the pulse amplitude.

The perturbation in the polymer structure between the domains results in a pressure acting on the domain wall. This force on a domain wall can be strongly reduced when it is compensated by free charges. The bound charges at the domain wall are screened and this reduces the energy of the depolarising field locally.

2.2. Semiconducting polymers

While many polymers are insulators, they can be semiconducting, if their backbone is conjugated. This means that it contains a structure of alternating single and double bonds. Due to the conjugation the carbon atoms show sp^2-hydridisation (figure 2.3 (a)). The $1s$ orbital is filled and only shown for completeness. In hybridisation the $2s$ orbital and two of the three $2p$ orbitals combine. They form three degenerate sp^2 hybrid orbitals. The third p orbital remains in its original state, which is higher in energy [22].

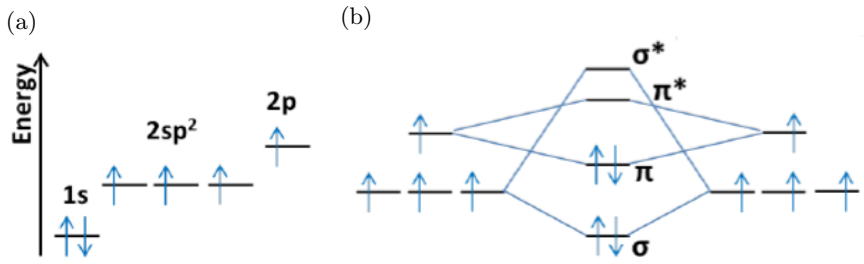

Figure 2.3.: **(a)** sp^2-hybridisation and **(b)** double bonds in ethylene showing only the valence electrons

Therefore in two carbon atoms forming a double bond (figure 2.3 (b)) each atoms is contributing three sp^2 orbitals and one p orbital. Overlapping orbitals will form a covalent bond. In the simplest example of ethylene (C_2H_4) two sp^2 orbitals for each carbon atom will overlap with the s orbitals of the four hydrogen atoms and form σ bonds. The remaining two sp^2 orbital form a σ bond between the two carbon atoms. The two p orbitals overlap and yield a so-called π bond.
The formation of the covalent bonds is described mathematically by the theory of the linear combination of atomic orbitals (LCAO). As can be seen in 2.3, the linear combination of two sp^2 orbitals gives two possible orbitals, the lower energy σ orbital and the higher energy σ^* orbital. Similarly the linear combination of the two p orbitals gives the possiblity of a lower energy π orbital and a higher energy π^* orbital. In a stable bond the lower energy orbitals σ and π are filled and the higher energy orbitals σ^* and π^* (called anti-bonding) are unfilled. Hence the π orbital corresponds to the highest occupied molecular orbital (HOMO) and the π^* orbital to the lowest unoccupied molecular orbital (LUMO).
Now considering a conjugated polymer all carbon atoms in the macromolecule have to be taken into account. The more carbon atoms contribute, the more the density

of energetic states increases and the distance between the HOMO and LUMO level decreases [23]. In a perfectly stretched macromolecule this would lead to formation of a valence and conduction band and the energy gap would be so small that the polymer would be a conductor. However the Peierl distortion in semiconducting polymers will always lead to a non-zero energy gap [24]. The macromolecule is never completely stretched out, so the conjugated π-electrons are limited to chain segments. The disorder also causes the charge carrier mobility in organic semiconductors to be orders of magnitude below that of crstalline silicone (about $1000\,\mathrm{cm}^2/\mathrm{V\,s}$) [25]. Due to the weak van der Waals forces between different macromolcules, the band width even in a highly ordered organic semiconductor is narrow.
One type of semiconducting polymer are polyfluorenes, which have a chain of benzene rings as the backbone. These conjugated polymers show electroluminescence [26, 27].

2.3. Thermally activated delayed fluorescence

Organic semiconductors are researched for the use in optoelectronic applications. One issue is their low external quantum efficiency (EQE). Electrical excitation typically results in 25% singlet excitons and 75% triplet excitons. However, the non-emissive triplet excitons do not contribute to the fluorescence of the material. After consideration of the light out-coupling efficiency the EQE is only as high as 5%.
One way to utilize the non-emissive triplet excitons is through thermally activated delayed fluorescence (TADF), which was first discovered in 1961 [29]. TADF is oxygen and temperature sensitive and can therefore be used in efficient optical sensors for these two parameters [28].
The transition of the singlet excitons with antisymmetric spin and a total spin quantum number of zero (S=0) to the ground state results in fluorescence and takes place within nanoseconds (this is called promote fluorescence (PF)). On the other hand the transition of the triplet state with even symmetry and S=1 to the ground state is quantum mechanically forbidden and results in phosphorescence with lifetimes of possibly seconds.

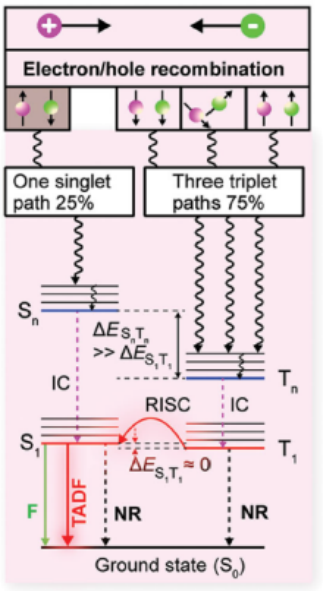

Figure 2.4.: Schematic of TADF (taken from [28]).

One way of harvesting the triplet excitons, that proofed efficient, is via the reverse intersystem crossing (RISC) process from the triplet state T_1 to the singlet state S_1 (see figure 2.4). According to Hund's rule, T_1 is always lower than S_1, so the RISC process has to be stimulated or activated. When the singlet-triplet energy difference is small, the endothermic RISC process can be overcome by the thermal motions of molecular atoms. The triplet excitons can be transformed into singlet excitons via

RISC and significantly enhance the luminescence through delayed fluorescence (DF). When TADF materials are excited both PF and DF can be observed with two different fluorescence lifetimes.

2.4. P(VDF-TrFE):PFO memory diode

In order to use as a memory diode thin films are produced from blends of the ferroelectric P(VDF-TrFE) and a semiconducting polymer processed from a common solvent (the process is described in 3.2.3). Here poly(9,9-dioctylfluorene) (PFO) is used as the semiconductor material. In the formation of the film the polymer blend decomposes by spinodal phase separation. In the ideal case this results in a microstructure of bicontinuous PFO domains in a matrix of P(VDF-TrFE). The blend film is sandwiched between two electrodes to create a two terminal device. The injecting electrode is chosen so that it forms a high-barrier Schottky contact with PFO. This results in the charge injection being limited. The diode is now in the high-resistance OFF state. When an electric field is applied and P(VDF-TrFE) polarises, the injection barrier is modulated and the resistance is lowered. The diode reaches the ON state. The reversible switching of the polarisation in the ferroelectric allows for switching between ON and OFF state of the diode.
The memory function is based on the hysteretic change in polarisation of the ferroelectric polymer. At low bias the current is injection limited. With increasing bias P(VDF-TrFE) gets polarised and above the coercive field E_c it is fully switched, which increases the current by orders of magnitude. Lowering the applied voltage again the polarisation remains and the diode stays in the ON state. In order to switch the polarisation again, one needs to apply a negative voltage larger than the coercive field.
In order to model the blend film in more detail [9] uses a two-dimensional model of columns of the two different polymers alternating. Upon polarising P(VDF-TrFE) a large stray electric field builds between the polarisation charges in the ferroelectric and the image charges in the electrodes. This lowers the energy barrier at the semiconductor-ferroelectric-electrode interfaces and enables charges to be injected in these areas. Here the injected charges change the semiconductor potential locally, which bends the electric field lines. There is no longer only a y-component of the polarisation in P(VDF-TrFE) along the direction of the external electric field, but the bending introduces a lateral x-component of the polarisation. This is compensated by further charge carriers accumulating at the PFO:P(VDF-TrFE) interface. Eventually an accumulation channel is formed throughout the whole height of the sample allowing charge to be transported from bottom to top electrode (see figure 2.5 for the depiction of the individual steps). Even though the x-polarisation is one order of magnitude lower than in y-direction, it is strong enough to maintain the accumulation channel (figure 2.6 (a) shows the importance of the x-polarisation for the device performance). At the top electrode, where the stray field has reversed orientation, the charges are pushed away from the interface, which leads to a pinch-off of the accumulation channel.

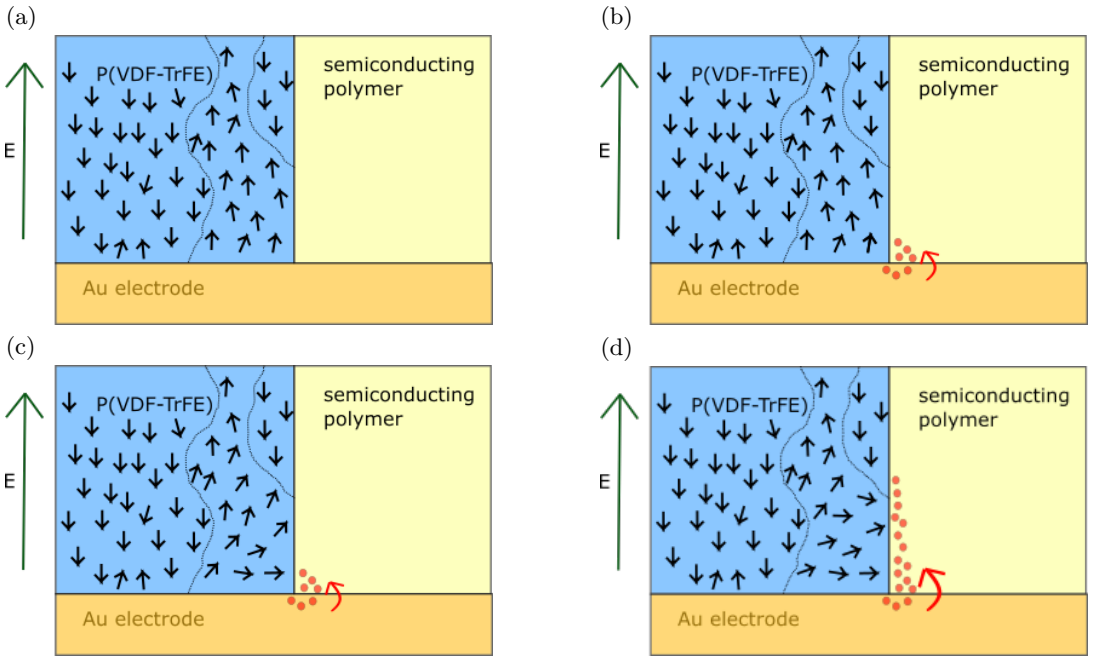

Figure 2.5.: Charge injection at the interface of the two components in the heterostructure and the electrode in a P(VDF-TrFE):PFO thin film device. Switching of domains (dipoles indicated by black arrows) upon application of an external electric field **(a)** induces large stray electric fields between polarisation charges and image charges in the electrode, which leads to a local lowering of the energy barrier at the interface and enables charge injection **(b)**. This introduces a x-polarisation component in the dipole orientation **(c)**, that is stabilized by further charge injection and accumulation at the ferroelectric:semiconductor interface **(d)**.

In the semiconductor the charge carrier density in the accumulation layer is four orders of magnitude higher than in the center of the columnar domain. The charge concentration already drops by a factor of 20 at a 2.5 nm distance from the interface with P(VDF-TrFE). Due to the small width of the energy barrier lowered by the stray field, the area of charge injection shows also a small depletion region of 3 nm. Both the charge injection and the charge transport are strongly space confined, which makes the memory diode an interface device.
The simulations also showed that the charge injection is dominated by tunneling. If tunneling is not taken into account the measured current cannot be explained well, while the model with tunneling describes the data perfectly (see figure 2.6 (b)). The tunneling rate is as high as $10^{26}\,\mathrm{cm}^{-2}\,\mathrm{s}^{-1}$ and therefore efficiently large to provide all the charges transported in the accumulated channel.

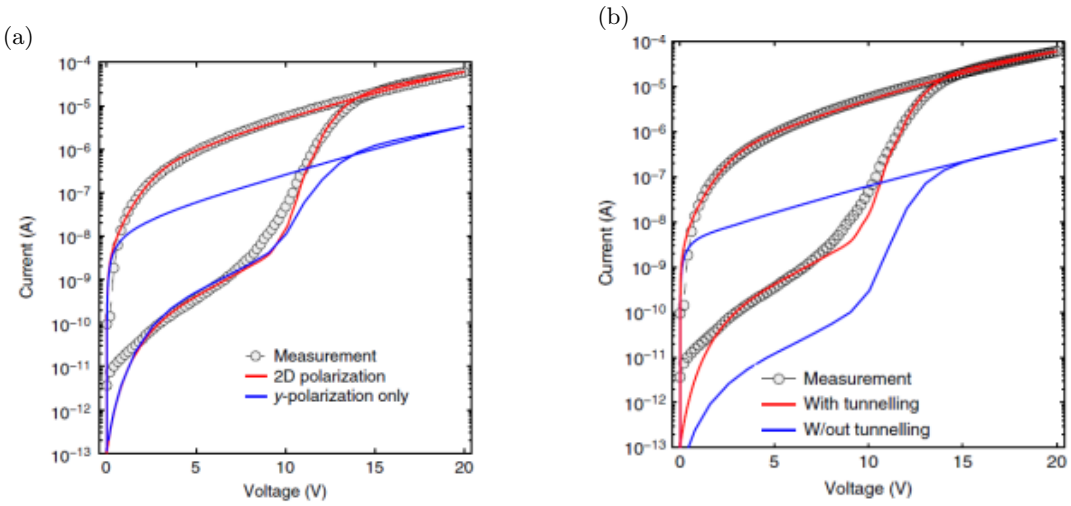

Figure 2.6.: Simulation results showing the significance of **(a)** 2D polarisation and **(b)** tunneling for the performance of the P(VDF-TrFE):PFO blend film device (taken from [9])

2.5. Breath figures

Generally the breath figure method utilises solvent-evaporative cooling on a solution surface under humid conditions. On the surface the water condenses and forms water droplets. After complete evaporation of the solvent the droplets remain in the film as pores. Polymer solutions are spin-coated under humid condition to create the porous films with thin and uniform thickness. The pore size formed by breath figures varies between a few hundred nanometers and several micrometers.
In [30] breath figures from a water-miscible solvent were first shown, when they demonstrated that tetrahydrofuran (THF) could also stabilise water droplets in the solution. The parameters, which influence the final outcome of the breath figure method, apart from the choice of solvent were discussed in [30] and [31]. They compared solutions of cellulose acetate butyrate (CAB) with different solvents. When using the water-immiscible chloroform the water droplets were very much stabilised in the polymer solution and created multi-layered pores in the upper part of the film, as well as a compact bulk layer of CAB below after full evaporation. Porous films being created with the water-miscible THF came unexpected as the solvent was considered to destabilize the water droplets. It can be explained by the fact that the liquids did not mix rapidly with each other and thus the water droplets decreased in size, but the process was stopped by the full evaporation of the solvent. It was also helped by the increased polymer concentration near the surface due to the fast solvent evaporation. This slowed down the intermixing between water and THF and made the solidification occur faster. After the film dried completely a layer of closely packed pores at the surface and randomly distributed pores of smaller diameter in the bulk of the film were observed (compare figure 2.7).

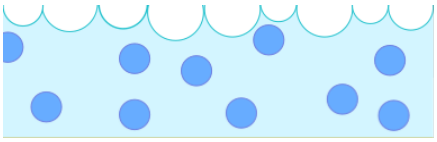

Figure 2.7.: Sketch of a typical breath figure pattern for water-miscible solvents.

The interfacial energy balance parameter z_0 determines whether it is possible to have condensed water droplets sinking into the film.

$$z_0 = \frac{\gamma_w - \gamma_{w/S}}{\gamma_S} \tag{2.1}$$

where γ_w and γ_S are surface energies of water and of the solvent and $\gamma_{w/S}$ the interfacial energy between water and the solvent. For $-1 < z_0 < 1$, water droplets are floating in polymer solution and only for $z_0 > 1$ droplets will sink. z_0 for water/THF solvent is estimated to be 2.76 with $\gamma_{w/THF} \approx 0$, $\gamma_w = 72.8\,\mathrm{mN/m}$ and $\gamma_{THF} = 26.4\,\mathrm{mN/m}$. So the negligible interfacial energy between THF and water lowers the energy barrier for nucleation of water droplets. A high interfacial energy between the two liquids would decrease the mixing in the bulk, but also lower the nucleation rate at the surface.
It has also been shown that the polymer concentration has an impact on the pore structure. For a low concentration in the solution the coalescence of water droplets can't be prevented because of the low solution viscosity and there is no formation of porous structures. On the other hand for a too high concentration the droplets are unable to sink into the solution and pores can only be formed on the surface.
The pores created by the breath figure method also strongly depend on the conditions during the spin-coating process. For evaporation under higher humidity levels the pore size was increased as larger water droplets condensed on the surface of the polymer solution. The rotation speed of the spin-coater also plays an important role for the final porous structure. For the experiments with THF it could be shown that under certain conditions all the pores in the bulk had a smaller size than the ones in the closely packed top layer, which indicates that the mixing of droplets with the solution is dominant over the coalescence of the droplets. This can be applied to produce more uniformly sized pores in the film.

2.6. Polarisation fatigue in P(VDF-TrFE)

Polarisation fatigue is limiting to the performance of a thin film device and was systematically studied for P(VDF-TrFE) in [32]. In those fatigue measurements using devices with gold electrodes a severe decrease in remanent polarisation could be seen upon continuous cycling of the device between OFF and ON state. Optical observation of the top electrode in micrographs showed the appearance of bumps (see figure 2.8).

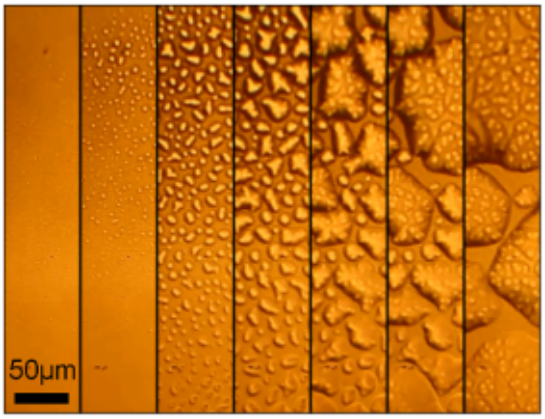

Figure 2.8.: In-situ micrographs of fatigue measurements of P(VDF-TrFE) showing the delamination of the gold top electrode (taken from [32]).

The fatigued strongly increased with increasing bias, as well as the number of switching events. It was seen that the higher the frequency of polarisation was, the faster was the degradation. It also depended on the applied waveform. Both the presences of injected charges and the switching of the polarisation were found to be prerequisites for fatigue.
In the search for the cause of the fatigue thermal stress could be excluded and piezoelectricity was ruled out. It is suspected that the origin of the delamination of the electrode are gases formed by phase decomposition of P(VDF-TrFE). Induced by high internal electric fields generated by polarisation switching, unzipping chain reactions occur, which release H^+ and F^- ions. The gold electrode is impermeable to the gases and acts as a barrier. The gas accumulates at the interface between P(VDF-TrFE) and the gold electrode and causes the bumps, that can be observed in the micrographs. The top electrode is delaminated, which can be observed by the naked eye.
It was shown that the endurance could be improved by exchanging the gold electrode for the polymeric conductor PEDOT:PSS, which is much better at releasing the gases. This improved the performance with respect to a gold electrode device, but still showed fatigue. Triangular or sinusoidal pulses yielded an improved endurance compared to the use of rectangular pulses, whose abrupt change in electric field causes stronger fatigue. When continuous cycling was interrupted every second with a waiting time of up to ten seconds, the cycling endurance increased with waiting time. During the waiting time the gases can diffuse out of the capacitor. Therefore the gas accumulation and degradation of the top electrode was prevented.

2.7. Basic neuromorphic terms

The attempt to achieve non-biological systems, which are acting like the basic components of the brain, i.e. neurons and synapses, is referred to a neuromorphic engineering. [33] gives a good overview of the basic terms from biology that are often used in

this context.
Elasticity is the ability to exhibit a restoring force against an external force. In this case the original state is recovered as soon as the external force is taken away. On the other hand plasticity refers to unrecoverable changes in the system. The external force is large enough to deform the system permanently. A sustainable change in state of a device is used for a memory function.
The neuron is a nerve cell consists of a lipid membrane that separates intracellular and extracellular media. This causes a discrete distribution of ions in the two media, which creates a potential. Therefore the cell membrane stays polarised with a particular resting potential, when it is in its resting state with no external potential applied. Ions can be exchanged between the intracellular and extracellular media through ion channels and ion pumps in the membrane. A voltage-spike travelling along a neuron's membrane, which triggers signal transmission between neighbouring neurons, is termed an action potential. The neurons are transmitting the action potential through them and are communicating with each other. Electric pulses are transported in a particular direction, so that the action potential transmission proceeds.

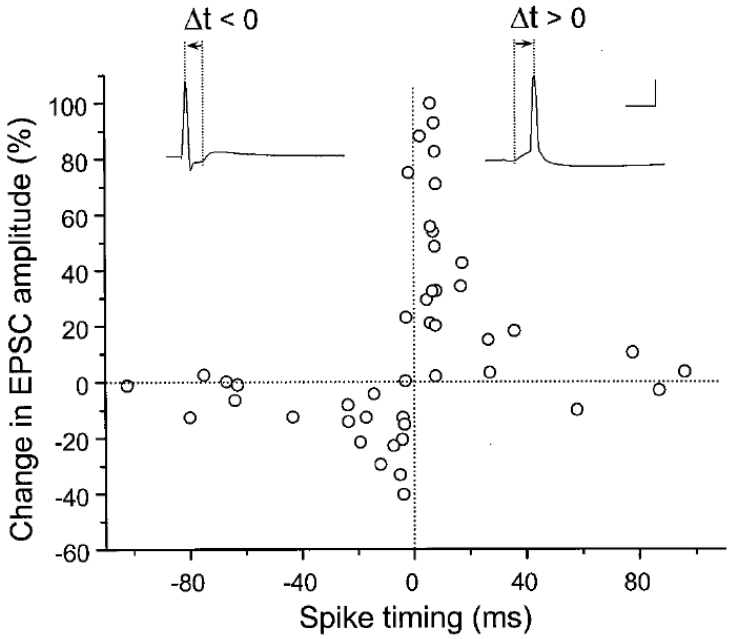

Figure 2.9.: Synaptic potentiation and depression (image taken from [34]).

The cleft between two neighbouring neurons, where those signals are transmitted, are referred to as synapses. In a chemical synapse the transmission takes place via neurotransmitters. The flow of neurotransmitters is unidirectional, so one can define a presynaptic neuron as a neuron releasing neurotransmitters and a postsynaptic neuron as a neuron receiving the neurotransmitters.
When external electric stimuli are above a certain threshold, a polarised nerve cell

at the resting state becomes depolarised. This depolarisation is termed as action potential firing. The over-threshold stimuli open the ion channels and the ions are redistributed to lower the chemical potential gradient between the intracellular and extracellular media. The depolarised state isn't kept for long, as ion pumps recover the ion concentrations of the resting state. Therefore the cell membrane state changes elastically.

Neighbouring neurons interacting by means of action potential transmission give rise to a change in synaptic weight. This change can last long showing plasticity, which is believed to be the source of memory and learning. An increase in synaptic weight is termed potentiation and decrease depression. Depending on the lasting time of the change in synaptic weight, these changes can be classified as short-term potentiation (STP) or depression (STD) and long-term potentiation (LTP) or depression (LTD). LTP is thought to be in charge of long-term memory and to take place, when both presynaptic and postsynaptic neurons are activated. A threshold of ion concentration has to be reached to result in LTP, otherwise the resting state is recovered and it exhibits STP instead.

Synaptic plasticity is timing dependent. The activation of both presynaptic and postsynaptic neurons does not necessarily lead to plasticity, but depends on the timing between the two voltage spikes. If it is outside a particular timing window, no lasting changes are imposed. This is referred to as spike-timing-dependent plasticity (STDP). When the time difference btw pre- and postsynaptic spike is less than approx. 20 ms, the synapse undergoes potentiation. Figure 2.9 shows the STDP researched by Bi and Poo in 1998.

3. Experimental

3.1. Materials

For the random copolymer of vinyldenefluoride and triflyoroethylene a composition of 75 mol% VDF and 35 mol% TrFE was used. It was bought from Solvay. For the production of the porous P(VDF-TrFE) thin films (see 4.1) P(VDF-TrFE) was dissolved in tetrahydrofuran (THF), which was purchased from Sigma Aldrich. The solution contained 1.5 wt% of the copolymer and was prepared by stirring at 70 °C.
The semiconducting polymer poly(9,9-dioctylfluorene) (PFO) was used to fill the porous P(VDF-TrFE) films (compare 4.1.4.1). It was synthesised in house and dissolved in toluene, that was purchased from Sigma Aldrich. Both solutions with 1.0 wt% and 0.5 wt% were used (see table 4.2), but the lower concentration was better suited.
The small molecule semiconductor 2,4,5,6-Tetra(9H-carbazol-9-yl)isophthalonitrile (4CzIPN), that emits photons trough TADF, was synthesised in house and also used to fill porous P(VDF-TrFE) thin films (compare 4.1.4.2). It was dissolved in chlorobenzene by stirring. Both 3 wt% an 1 wt% solutions were used in spin-coating (see table B.3) and a 1 wt% solution in bar-coating.
A blend solution of P(VDF-TrFE) and PFO was used as well. Therefore the polymers were mixed in a 9:1 ratio (27 mg P(VDF-TrFE) and 3 mg PFO) and dissolved in 1.5 mL THF to produce a 2 wt% solution. It dissolved under stirring at 80 °C and was filtered with a 1 µm PTFE filter.

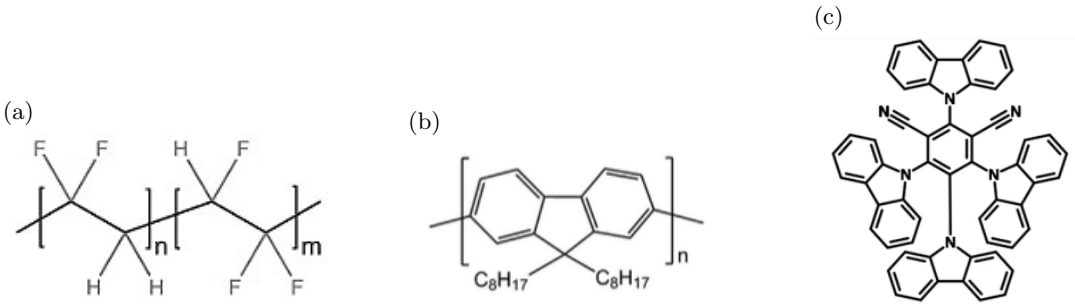

Figure 3.1.: Chemical structure of **(a)** P(VDF-TrFE), **(b)** PFO and **(c)** 4CzIPN.

Quadratic glass slides of 9 cm^2 area (Schott Borofloat 33) were used as substrates. They were manually cleaned in warmed water with soap (Extran MA 02 from Merck Milipore). Afterwards followed a ultrasonic treatment in deionized water, acetone, and 2-propanol. Then the glass substrates were subjected to UV/ozone treatment

(UVOCS) to remove any residues. Electrods were thermally evaporated onto the glass substrates through shadow masking. Chromium (1 nm) served as the adhesion layer for gold bottom electrodes. For the first project (section 4.1) 20 nm of gold were used for the bottom electrode and 5 nm barium and 100 nm aluminium as the top electrode. The second project (section 4.2) had a symmetric structure with 50 nm of gold for each electrode.

3.2. Device fabrication

3.2.1. Fabrication of porous P(VDF-TrFE) thin films

For the fabrication of the porous ferroelectric thin film of P(VDF-TrFE) the breath figure method under a controlled humid atmosphere was applied (see experimental section 2.5). A LabSpin6 TT spin-coater from Suss MicroTec placed in normal ambient conditions in a laboratory environment was used. The cleaned glass substrate with bottom electrodes, consisting of an adhesion layer of 1 nm chromium and 20 nm gold evaporated onto it, was placed on the chuck inside the spin-coater and fixated by a vacuum during the spinning. Since the conditions during the spin-coating process were determining for the pores, that could be produced, measures were taken to control the atmosphere inside the chamber of the LabSpin6 TT. This way the thin films became reproducible by excluding the changing ambient conditions.

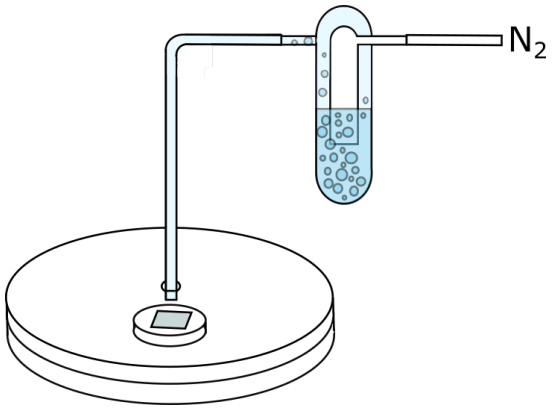

Figure 3.2.: Illustration of the set-up used for controlling the conditions inside the spin-coater. A humid nitrogen flow through a gas bubbler with warmed water was created to fill the chamber surrounding the sample.

A gas bubbler, containing water warmed to 100°C, was attached to a nitrogen source to create a humid nitrogen flow (compare figure 3.2). The chamber was first filled up with nitrogen. A humidity sensor inside the chamber was used to monitor the atmosphere. A fast filling of 3-5% humidity decrease per second was fine for this part. When the sensor showed a very low humidity level, due to the ambient atmosphere having been replaced by nitrogen, the humid nitrogen flow was attached. The chamber

was slowly filled until the desired humidity level was reached. This was varied between 50% and 80% humidity.
The rate at which the humidity inside the chamber increased was adjusted with the pressure of the nitrogen tap and measured with the sensor. It showed to be very important to control this rate precisely. An increase in humidity of 0.3-0.5% per second was ideal. A faster increase would lead to large water droplets, that form pores with diameter larger than 1 µm, condensating on the glass plate. On the other hand a slower rate could allow the ambient conditions to fill the chamber again through gaps.
When the humidity level was reached, the solution containing P(VDF-TrFE) dissolved in THF was deposited onto the substrate in the spincoater chamber through a hole in the lid. Without delay after the deposition the hole is closed off and the spinning was started. It was spin-coated for 30 s at a speed of 1000 rounds per minute (rpm). The hole in the lid was closed until the spinning had stopped.
The humidity sensor showed some decrease during the 30 s spinning, so the stability of the created atmosphere was examined by filling up the chamber regularly and then just closing it off and observing the humidity for 30 s. The humidity level stayed constant, so the decrease was due to the spinning motion affecting the sensor.
The P(VDF-TrFE) thin films were heated in a vacuum oven at 160 °C for different amounts of time (between 10 and 45 min). In this step it was important again to control the atmosphere inside the oven, as ambient conditions influenced the result negatively.

3.2.2. Fabrication of memory diodes

For the production of memory diodes bottom electrodes, consisting of an adhesion layer of 1 nm chromium and 20 nm gold, were evaporated onto cleaned glass substrates. Afterwards the porous P(VDF-TrFE) thin films were processed as described above. For these samples the spin-coater was filled to a humidity level of 80% and the thin films of P(VDF-TrFE) were heated for 35 min for the heating process (see 4.1 for the measurements of the humidity and heating time dependency, after which these parameters were chosen). Afterwards the samples were annealed at 130 °C for 2 h under vacuum conditions.
In order to fill the pores in the thin film with PFO as the semiconductor spin-coating was applied again. Here another LabSpin6 TT spin-coater placed in the nitrogen atmosphere of a glove box was used. All devices were spin-coated for 30 s, while the speed was chosen individually for each sample (refer to chapter 4.1.4.1 for the discussion and all details). Heating the PFO solution to 70 °C also proved useful in dealing with problems in filling the pores with the semiconductor material without creating a high add layer on top of P(VDF-TrFE).
When 4CzIPN was used as the semiconducting material spin-coating with different speeds was applied again. It was also attempted to improve the wetting of the surface by treating the surface of the porous P(VDF-TrFE) before 4CzIPN was spin-coated on top of it. The time delay between the surface treatment and the spin-coating

was kept as short as possible (a few minutes until the sample had been brought into the glove box equipped with a spin-coater). One sample was subjected to 1 min of UV/ozone (UVOCS). Two other samples were treated with oxygen plasma (100 W, 5 s) and nitrogen plasma (100 W, 5 s) before 50 µL of the 4CzIPN solution was deposited for spin-coating.
Additionally for 4CzIPN the wire-bar coating technique was applied. A K202 control coater (RK PrintCoat Instruments Ltd, UK) with a bar with a close wound 0.05 mm thick wire (white bar) was used. The glass substrate was placed onto the heated metal board and two empty glass slides on either side of the sample were used to keep the bar level. The 4CzIPN solution is deposited just before the wire bar and the automated movement with constant speed is started to spread the solution equally over the sample area. Different heating temperatures and solution volumes were tested (see table 4.3).
Afterwards the top electrode was produced by evaporating 5 nm of barium and 100 nm aluminum onto the phase-separated film.

3.2.3. Fabrication of P(VDF-TrFE):PFO blend film devices

To create the blend film devices of P(VDF-TrFE) and PFO for the measurements of multilevel switching behaviour, both polymers were spin-coated from a common solvent (see 3.1 for details of solution preparation). The blend solution dissolved in THF was spin-coated onto a cleaned glass slide with bottom electrodes (1 nm Cr, 50 nm) under nitrogen atmosphere inside the glove box. The pattern for the electrodes were five parallel lines of 400 µm width.
Two samples were coated with the blend film. Both were spun for 30 s at 750 rpm and 500 rpm respectively. The faster spin-coating speed resulted in a film thickness of (211.8 ± 16.3) nm and 500 rpm in (258.8 ± 5.3) nm.
Afterwards the dried thin films were annealed at 140 °C for 90 min. For the top electrodes 50 nm of gold were evaporated using the same masks, but now turned 90°, so that an array of 25 device each with an area of 0.16 mm^2 is made. The bottom and top electrode are therefore of the same material and thickness and the device structure is completely symmetric. For individual measurements the single devices were disconnected.

3.3. Structural characterisation

Atomic force microscopy (AFM) was carried out with a Nanoscope Dimension 3100 from Bruker using tapping mode. In the measurement the surface of the sample is scanned with a tip mounted on a cantilever. By focusing a laser beam on the back of the cantilever and the reflected beam being measured by a photodiode sensor, the movement of the tip above the surface is recorded. The height of the tip is adjusted, so that the amplitude of the potential between the tip and the surface is kept constant. While scanning over the sample at a typical scan frequency of 0.5 Hz, a feedback loop moves the cantilever up and down with a piezoelectric element. The captured height

data was processed using the Gwyddion software. An overview of the technique can be found in [35] and an example of an image captured with AFM can be seen in figure 4.5.

Surface profilometry measurements were performed with a Dektak XT from Bruker. The thin films were scratched in a small line down to the surface of the glass slide to measure the film thickness. The lever of the profilometer was moved in an automated motion orthogonally to the scratch to capture the height difference. After levelling the height measured on both sides of the scratch and the difference between this surface of the film and the surface of the glass substrate, the film thickness could be determined.

Scanning electron microscopy (SEM) using the a Hitachi SU8000 was performed by Gunnar Glaßer. The low energy secondary electron (SE) top detector at a x1.00k magnification was used to take the images for the statistical analysis of the porous P(VDF-TrFE) films (see figure 4.4). To image the surface topography in more detail both SE and the high energy back-scattered electrons (BSE) in the upper detector were used at a x10.0k magnification (compare figures in 4.3 and B.3).

3.4. Image analysis

In order to use the SEM images for statistical analysis of the porous P(VDF-TrFE) thin films a MATLAB program was written, which can be found in appendix B.1. For each sample four SEM images with x1.00k magnification, taken in different areas of the sample, were transferred into a black and white image and loaded into MATLAB. The programm was used to set the correct scale, find circular pores and determine their diameter and area. Then the total area of all pores found in the images was calculates and with it the ratio between pore area and total image area. This was done for all four images and the average area ratio calculated. All detected pore diameters of all four images were collected and a histogram plotted. The normal distribution was fitted to this histogram to determine the average pore diameter over the whole sample area. The differences in the area ratio and average diameter determined for each image, depicting a certain area of the sample, was always very close to the values in a different image of another area of the sample. The samples displayed equal distribution of pores.

3.5. Electrical characterisation

The efficiency of the memory diodes produced with the backfilled pores method was calculated after measuring the light and current output of the device. The set-up was placed under glove box atmosphere and used a Keithley 2400 source meter controlled by a LabView softare for the current measurement. The photocurrent was measured using a calibrated Si photodiode. For the measurements the voltage was swept from 0 V to 2 V, then lowered to −2 V and increased again to 0 V. This was repeated

with the maximum voltage increased by 2 V each time (±4 V, ±6 V, ..., ±20 V). An example of 20 V sweep is discussed in 4.1.4.1 for figure 4.8.
The blend film memory diodes for multilevel switching were analysed with a Keithley 4200-SCS Parameter Analyser. The voltage was applied and the current measured for a sample placed on a probing station inside a vacuum chamber under 1×10^{-5} mbar. The I-V sweep measurement with continuously increasing voltage were made using the SMU of the Keithley, which allowed for high resolution even for the low current values of the high resisitance OFF state.
The KITE program used with the Keithley 4200-SCS allowed with the Segment ARB waveform option to define a customized pulse train by controlling the pulse width and amplitude of each pulse, as well as the time between pulses of up to 40 V and as short as 40 ns. The program is used with a PMU, which is able to both apply the pulses and measure the current output. Since it was observed that the use of the PMU could not resolve the low current output (see 4.2.2), Segment ARB and the PMU was then only used for programming the device and not read-out. The two channels of the PMU can apply independently defined pulse trains.
One set-up used to for the read-out operation was a combination of a current preamplifier (Stanford Research Systems Model SR570 Low-Noise Current Preamplifier) and an oscilloscope with high sampling rate (Agilent Infinii Vision DSO-X 3012A Digital Storage Oscilloscope). After it was seen that the fast read-out was problematic (see 4.2.2), voltage sweeps with the SMU of the Keithley 4200-SCS were used for slow read-out.

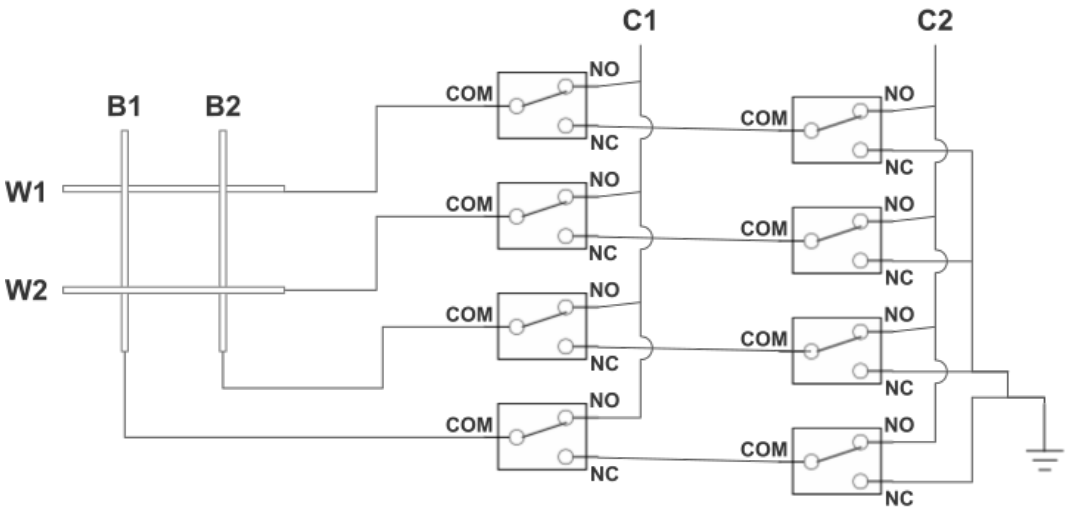

Figure 3.3.: Switch board set-up to select which line in the array the voltage signal from channel 1 (C1) and channel 2 (C2) of the Keithley 4200-SCS is applied to, as well as which are grounded.

For the measurements on a 2x2 array of memory diodes a switch board shown in figure 3.3 was used. Four switches each were used to select which of the four lines of the

array were connected with channel 1 or channel 2 of the Keithley. It was always chosen such that one line was connected to channel 1 and an orthogonal line to channel 2, so that the full voltage difference was applied to the selected device in the array, and the other lines were grounded.

4. Results and Discussion

4.1. Porous P(VDF-TrFE) thin films with 3-1 connectivity for phase separated heterostructures with improved morphology used in memory diodes

As described in the introduction the common method used to produce phase separated heterostructure thin films of P(VDF-TrFE) and PFO doesn't result in the ideal morphology needed for the memory diodes. So instead it was proposed to create a P(VDF-TrFE) thin film with bicontinuous columnar pores, which can be backfilled with a semiconducting material. This method promises to have all semiconductor material in a continuous domain in contact with both bottom and top electrode and therefore contributing to the device performance.
As described in 3.2.1 the general idea was to get the desired porous films by using the breath figure method to have pores in the spin-coated films and then heat the samples to form out columnar pores.

4.1.1. First attempts in the search for porous P(VDF-TrFE) thin films

The requirements for the ideal result were set by what had been determined to be the best in the experiments with samples created with the common blend film method. For those the use of a 1:9 PFO:P(VDF-TrFE) polymer blend was ideal, which would result in about 10% of the area in a top view of the thin film consisting of the semiconductor material. It has to be taken into account, that as described in 1 only a certain amount of the PFO was in electrically functional domains (about two thirds). Therefore it was aimed to also have around 6 to 7% of the area of the P(VDF-TrFE) thin film covered with pores, which will eventually be the semiconductor domains. For the pore diameter a size of 400 nm to 500 nm was used.
In the first attempts to create a porous P(VDF-TrFE) thin film a solution of the polymer in THF with water added to it was used comparable to the experiments in low humidity conditions described in [30]. There they used the water content in there solution to control the pore size of their breath figure film. It was thought that this method could be used here as well to produce the desired porous P(VDF-TrFE) thin films. In the later, successful samples this method was no longer applied, because the humidity in the spin-coater was regulated instead.
These early experiments showed the importance of controlled conditions during the production process. For these samples heating was not conducted under vacuum yet, which influenced the results due to the varying ambient conditions in the oven. Even

though this lead to a larger spread in pores diameter and the appearance of pore clusters in the film, rather than completely randomly distributed pores (see figure 4.1), these measurements helped to determine the dependency on the heating time and humidity levels during the spin-coating process.
In general the two parameters, by which the films were characterised after imaging with SEM, were the pore diameter and the ratio between area covered by pores and total area (see figure 4.2). Those influence the size of the semiconductor domains and the ratio between ferroelectric and semiconducting component in a backfilled film respectively.
In early porous P(VDF-TrFE) films, which were created by spin-coating under ambient conditions, the dependency on the heating time, also in ambient conditions, was researched. Samples were prepared under the same conditions and then heated for 5, 15, 30, 45 and 60 minutes. While after 5 minutes only about 0.8% of the area was occupied by pores, it increased to 17.6% for the 60 minutes sample. There was also an increase in pore diameter from around 700 nm to around 900 nm visible with a wide spread in the diameter (compare table B.1).

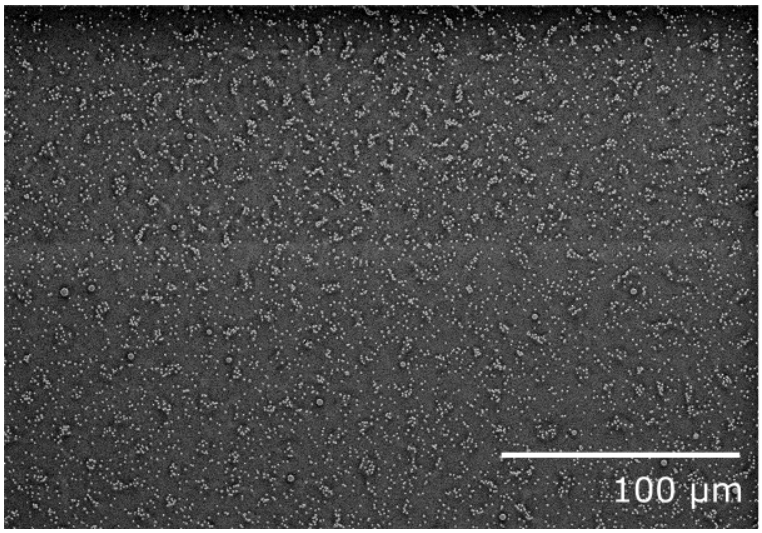

Figure 4.1.: Porous P(VDF-TrFE) film produced at 60% humidity in the spin-coater under not yet optimized conditions in the early measurements and heated for 20 min. Images for 50%, 70% and 80% humidity can be found in the appendix in figure B.1.

A next series of measurements was now conducted under the controlled atmosphere described in the experimental section 3.2.1. The thin films were spin-coated under 50%, 60%, 70% and 80% humidity. All samples were heated for 20 minutes. Especially for the samples produced under higher humidity environment the SEM images showed clustering of pores (compare figure 4.1 and B.1). This indicates that the correct parameters for controlling the atmosphere in the spin-coater hadn't been found yet and this was no longer a problem in the improved later samples. The results in figure

4.2 show the general trend of both the area ratio and the average pore diameter increasing with the increased humidity. While the sample spin-coated under 50% humidity showed 1% pores, it increased to 17.6% for the 80% humidity sample. The pore diameter increased from around 600 nm to 800 nm (compare also table B.2). From the SEM images it appeared that for high humidity the pores didn't just cluster, but actually coalesced, which affected the average diameter. For well distributed pores in the improved samples, this was no longer observed.

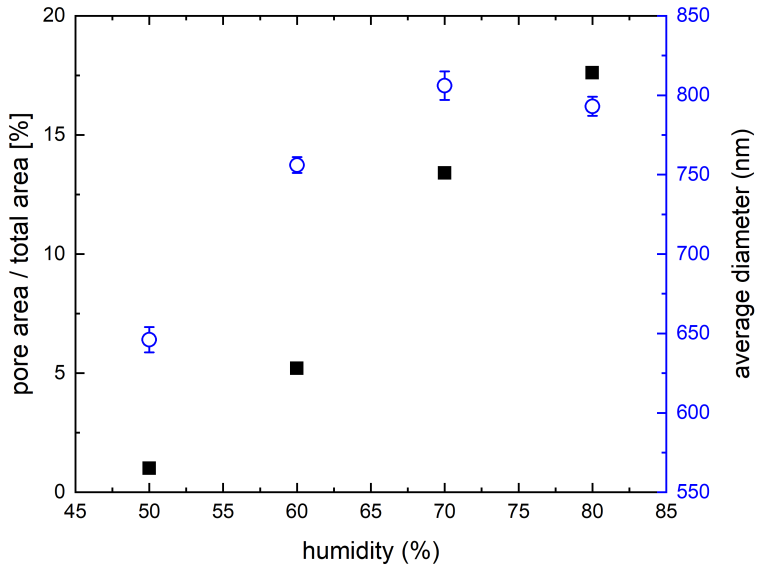

Figure 4.2.: Measurement of the pore area to total area ratio and the average pore diameter dependent on humidity level during the spin-coating process of the P(VDF-TrFE) thin films.

4.1.2. Analysis of the porous P(VDF-TrFE) thin films created by increasing heating time

After improving the method by finding the correct parameters for controlling humidity levels in the spin-coater (compare description in 3.2.1) to avoid clusters of pores or larger pores and using a controlled atmosphere in the vacuum oven as well, new samples were analysed for the heating time dependency. All samples were spin-coated under 80% humidity. While one sample was kept pristine for comparison, the others were heated for 5, 10, 20, 25, 30, 35, 40 and 45 minutes respectively at 160 °C.

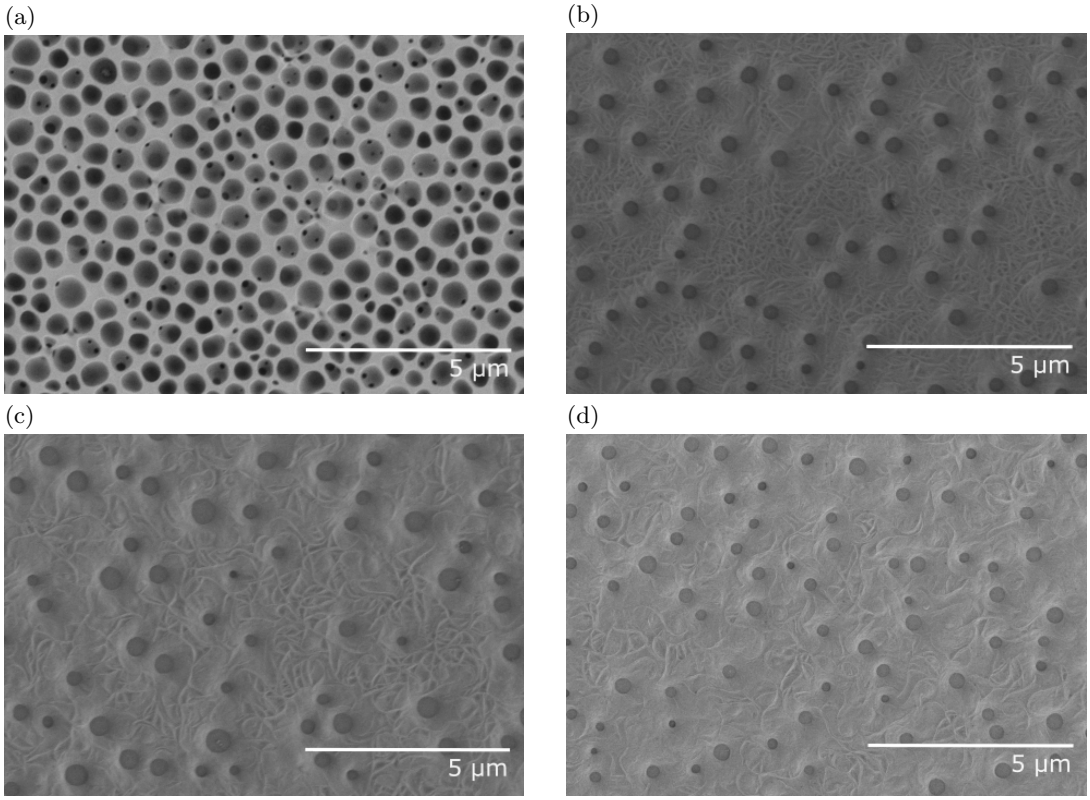

Figure 4.3.: SEM images of porous P(VDF-TrFE) films with different heating times in the vacuum oven after the breath figure spin-coating of the solution. Figure **(a)** shows a pristine film after spin-coating, while the other samples shown here were heated for **(b)** 10 min, **(c)** 25 min and **(d)** 40 min. Additional samples can be seen in the appendix B.3.

4.1.2.1. SEM imaging for analysis of pore density and diameter

Imaging with the scanning electron microscope allowed for analysis of the development of the pores. Figure 4.4 shows well distributed pores for the sample heated for 30 min and the inset histogram shows how the diameters are now following the normal distribution. Previously, with the larger pores appearing on the films, the distribution had always been asymmetrical towards the larger diameters. This shows that the process is now controlled enough to produce reliable samples without visible defects. For each sample four images at this magnification were taken and used for statistical analysis of the pores.

More close-up SEM images of each sample with different heating times allowed the observation of structural changes in the porous polymer films. Figure 4.3 (a) shows the sample, which was not heated and therefore has the typical breath figure structure. Close-packed pores with shallow depth (visible through the smaller and deeper areas within them) can be seen. For the sample heated for 10 min (4.3 (b)) the structural

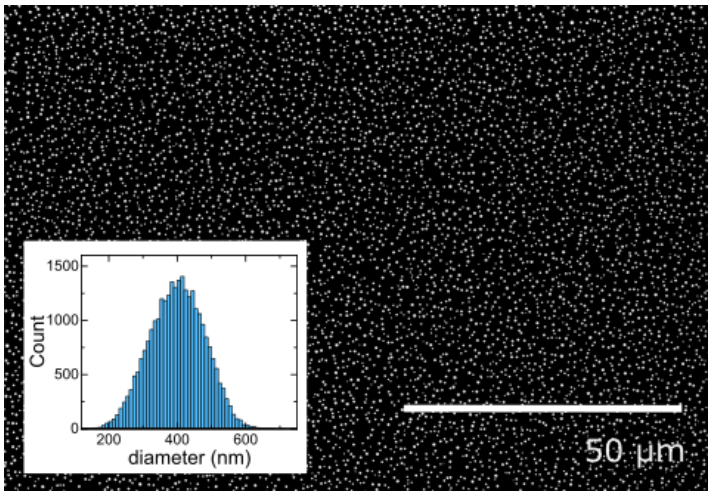

Figure 4.4.: Porous P(VDF-TrFE) thin film produced at 80% humidity and heated for 30 min shows well distributed pores with the diameters well distributed.

change was already clearly observable. The close-packed pores can no longer be seen, but instead deeper pores of smaller diameter. The bottom of the pores appears to be even. The surrounding polymer shows the thread-like polymer pattern. Looking at the sample heated for 25 min 4.3 (c) the polymer structure is already slightly changed and after 40 min of heating 4.3 (d) there is more "softening" of the polymer structure visible. Additional images of the other samples can be found in the appendix (figure B.3).

4.1.2.2. AFM imaging for analysis of pore depth and measurement of film thickness with DEKTAK profilometer

AFM imaging was additionally used to determine pore depth and validate the impression of increasing depth from the SEM imaging. After scanning the sample surface with the AFM tip depth profiles were used to determine the pore depth (see an example in figure 4.5). For the pristine film, that was not put in the vacuum oven, the pore depth measured was 30 nm to 40 nm, which fits the expectation of a layer of shallow pores at the surface of a typical breath figure structure for water-miscible solvent. It also matches the impression of the SEM images at higher magnification. For the sample heated for 10 min a pore depth of 40 nm to 60 nm was measured. The P(VDF-TrFE) thin films heated for 20 min or longer all had a pore depth of 100 nm to 120 nm.
The measurement of the film thickness with the DEKTAK profilometer showed a higher thickness of 152 nm, while all heated films had a film thickness around 120 nm. All data collected from SEM and AFM imaging and the profilometer can be found in table 4.1.

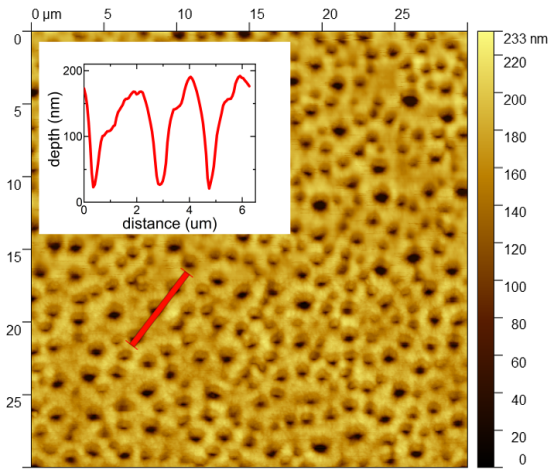

Figure 4.5.: Exemplary AFM image of a porous P(VDF-TrFE) thin film for analysis of the pore depth. This was the sample heated for 30 min.

heating time [min]	film thickness [nm]	pore depth [nm]	average pore diameter [nm]	ratio pore area to total area [%]
pristine	152	30-40	508	-
10	120	40-60	407	-
20	125	100-120	325	4.24
25	118	100-120	408	5.41
30	128	100-120	400	6.89
35	122	100-120	472	10.91
40	113	100-120	376	6.06
45	116	100-120	404	5.77

Table 4.1.: Overview of all data on the porous P(VDF-TrFE) thin films heated for increasing amounts of time collected from SEM and AFM imaging and the thickness measurement with the profilometer. Area ratio was only calculated for the fully formed pores of 100 nm to 120 nm depth.

4.1.3. Porous P(VDF-TrFE) thin films with 3-1 connectivity

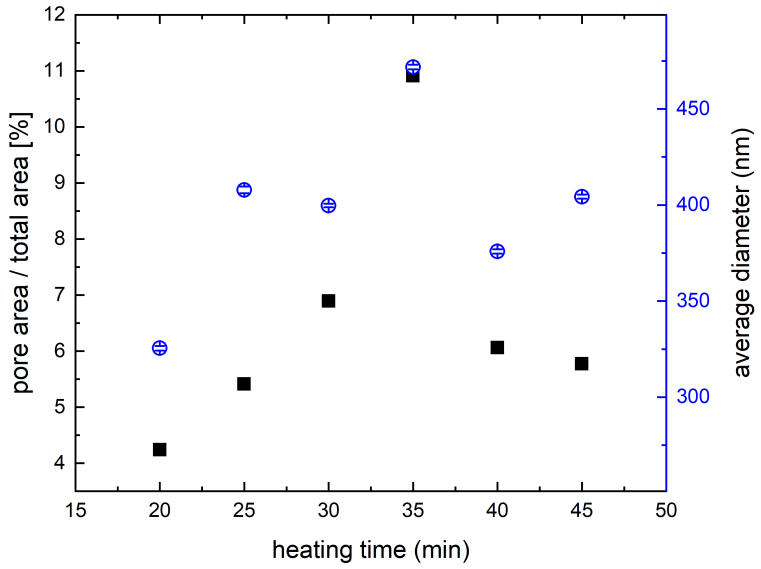

Figure 4.6.: Heating time dependency of the average diameter and density of pores in the P(VDF-TrFE) thin films produced with breath figure method under humid condition (80% humidity). Values were taken from the statistical analysis of SEM images.

Taking into account the measured film thickness and pore depth, all samples heated for 20 min or longer showed bicontinuous pores. Therefore for these samples the ratio between pore area and total area observed was calculated, since for the continuous columnar pores this directly relates to the ratio between the two polymer material in the backfilled device. In figure 4.6 one can observed how this ratio increases between heating times of 20 min to 30 min and then stagnates around 6%. Similarly the average diameter can also be seen to increase with heating time, but then continue around 400 nm. Both parameters have an outlier for the 35 min sample, which speaks for this particular sample being affected by some irregularity in the production process.
Taking together all the data retrieved and considering the different samples as snapshot during the heating process, a sketch of the pore development during the heating was developed (see figure 4.7). After the spin-coating in humid atmosphere and the complete evaporation of the solvent the water droplets leave spherical pores in the polymer network of P(VDF-TrFE) (4.7 first image).
Heating the sample in vacuum to 160 °C brings the polymer from the rubbery state to the rubbery flow. This softening of the surrounding network allows the water droplets to evaporate, which leaves a columnar pore in the thin film.

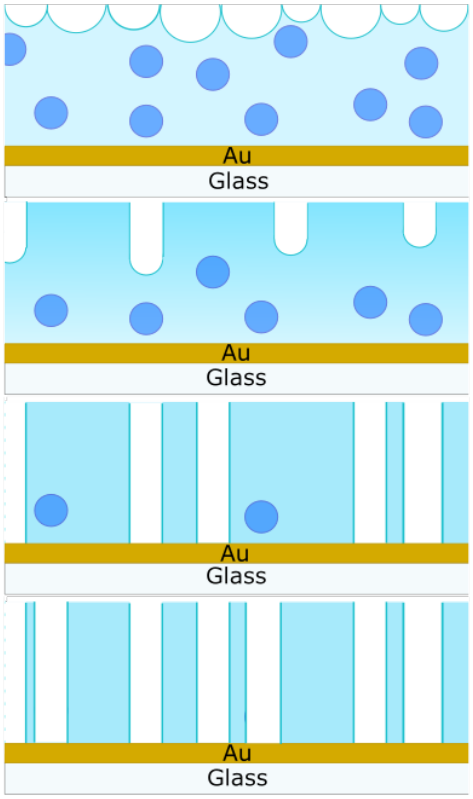

Figure 4.7.: Sketch of the pore development in the thin films with increasing heating time.

The temperature was chosen such that the water escapes the film into the atmosphere above, rather than a pore to coalesce with other pores near it. At higher temperatures and therefore stronger softening of the polymer network coalescence would play a role and influence the pore diameter obtained. Due to the gradual heating of the film the columnar pores will first appear close to the surface, which can be observed in the shallower pores in the film after short heating times (4.7 second image). This corresponds to the pores observed after 10 min of heating time. Additionally between these two samples a lowering of film thickness by 30 nm and the disappearance of the close packed surface pores was observed. The film thickness measured for the pristine P(VDF-TrFE) thin film, determined with a DEKTAK surface profilometer, was 152 nm and for all samples, which had been heated for at least 10 min, the film thickness was (120 ± 10) nm. No change in thickness was seen apart from a reduction in the first minutes of heating (see also table 4.1), which indicates that the shallow pores on the surface evened out upon the first minutes of heating.

For heating times of 20 minutes and longer all pores were 100 nm to 120 nm deep and therefore bicontinuous through the film. This variation in pore depth is shown in figure 4.7 in the third picture. For continued heating of the polymer the pores are further formed and reach 3-1 connectivity. In the AFM analysis continuous pores were first observed after 20 min heating time. Looking at figure 4.6 it can be seen that the number of pores still increases up to 30 min of heating time, while the maximum diameter of 400 nm is already reached after 25 min. Therefore it can be assumed that between the 20^{th} and 30^{th} minute more pores are formed until the final state is reached (figure 4.7 last image). It has been shown that the pores will not change anymore afterwards (figure 4.6).

4.1.4. Filling the porous P(VDF-TrFE) thin films with semiconducting polymer

In order to create the phase separated thin films for MEMOLED devices, the porous ferroelectric film were filled with a semiconductor material. First the P(VDF-TrFE) films were produced according to the description in the experimental section 3.2.1 and heated at 160°C for 35 minutes to ensure the continuity of the pores. Afterwards the samples were annealed at 130°C for 2h.

4.1.4.1. PFO as the semiconductor material

First the semiconducting polymer PFO dissolved in toluene (see 3.1 for details) was used with the porous P(VDF-TrFE) thin films. The solution was deposited on porous P(VDF-TrFE) thin films and spin-coated under nitrogen atmosphere. Table 4.2 shows different attempts to fill the pores properly with the semiconductor material without creating a high add layer on top of P(VDF-TrFE). An add layer beyond a certain thickness will influence the device performance negatively. After the spin-coating process a top electrode was evaporated onto the sample (compare 3.2.2). The devices were evaluated by simultaneously measuring the current and photocurrent output, while sweeping the voltage with increasing amplitude. Additionally all samples were imaged with AFM to show the distribution of PFO on the porous films and measure height differences on the sample. Thickness measurements determined the add layer thickness.
Different observations could be drawn from various PFO devices (shown in table 4.2). The maximum value in current measured was directly dependent on the thickness of the add layer. For an increase in add layer thickness the maximum current value decreased. This was especially a problem with the first device described in the table, which had a very thick add layer. Therefore for the following devices the solution concentration was reduced.
For devices with the pores filled less than two thirds of the height (less than 80 nm out of the 120 nm total film thickness) the current curve didn't have the espected shape seen in figure 4.8, but instead already showed very high current output for low voltages applied and then normalised more at higher voltages. The desired hysteresis could not be observed. This problem was for example seen for the second and third device in the table.
To fill the pores up more the spin-coating speed was reduced for the forth device (table 4.2). This lead to the observation of a correct hysteresis loop, but this device showed a low photocurrent output, so the result wasn't ideal yet. For device 5 the attempt was made to fill the pores better with the PFO semiconductor by having a delay between the deposition of the solution onto the porous P(VDF-TrFE) film and the starting of the spin-coater, but this was not successful.
An improvement could be made by heating the PFO solution to 70 °C before the deposition. This overall increased the PFO thickness, both in the pores and the add layer (compare device 2 and 6 in table 4.2). When additionally the spin-coating speed

	PFO conc. in solution [wt%]	spin-coating speed [rpm]	comment	PFO level in pores [nm]	add layer thickness [nm]
1	1.0	1000	annealed after filling	completely filled	100 to 120
2	0.5	1000	annealed after filling	40 to 60	10 to 20
3	0.5	1400	annealed after filling	40 to 60	10 to 20
4	0.5	750	annealed before filling	80 to 90	30 to 40
5	0.5	1000	annealed before filling, 25s delay between solution deposition and spin-coating	20 to 30	20 to 30
6	0.5	1000	annealed before filling, solution heated to 70 °C	65 to 75	25 to 35
7	0.5	750	annealed before filling, solution heated to 70 °C, slow deposition of solution	completely filled	80 to 90

Table 4.2.: Overview of different P(VDF-TrFE):PFO heterostructure devices.

was reduced, the pores could be filled completely and the good performance of device 7 (shown in 4.8) could be measured.
The device shown in figure 4.8 has the expected MEMOLED behaviour. The current measurement displays a hysteresis loop and the photocurrent increases dependent on the current level. Photons are first emitted, when the current reaches a value of around $1\,A/m^2$. The photocurrent increases more than two orders of magnitude and also shows the hysteresis, proofing that it is directly related to the current through the P(VDF-TrFE):PFO device.
Now the efficiency, which is the ratio between the photocurrent and the current, of the device produced by the new method was compared to a published result for a device processed in the common way from a blend solution. In figure 4.9 it can be observed that the new method presented here resulted in improved device efficiency by about one order of magnitude.

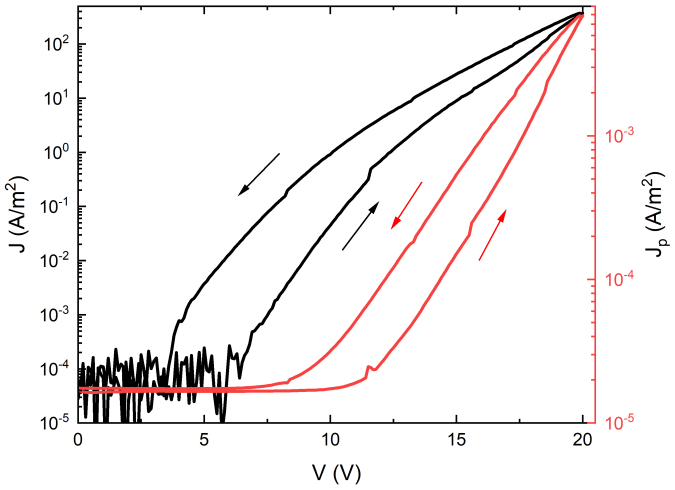

Figure 4.8.: Current and photocurrent measured for device 7 from table 4.2, which shows the expected MEMOLED performance. The current shows the hysteresis of the ferroelectric and the semiconductor PFO will emit photons, when the current is sufficiently high.

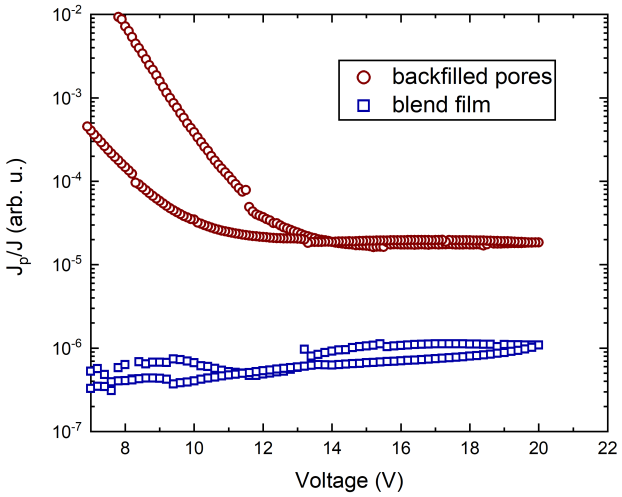

Figure 4.9.: Efficiency of the backfilled device, prepared with the process described here, in comparison with a common blend film device of P(VDF-TrFE) and PFO.

4.1.4.2. 4CzIPN as the semiconductor material

After P(VDF-TrFE):PFO memory diodes were realised, it was attempted to use the advantage of this method it be able to fill the created pores with different semiconductor materials. Hence the same spin-coating process was used with 4CzIPN dissolved in chlorobenzene (see experimental section 3.1 for details). This showed that the difficulty with the small molecule semiconductor solution was in creating a film that would cover the whole surface of P(VDF-TrFE) equally. For many devices the films of 4CzIPN seen in AFM analysis were not continuous, but only certain areas of the device had 4CzIPN in the pores and as an add layer on top of P(VDF-TrFE). Other areas didn't have any 4CzIPN, whether in the pores (for which still the original thickness was measured) nor as an add layer.
Figure 4.10 (b) depicts this observation. In comparison with 4.10 (a) can be seen that the uncovered area is not filled with 4CzIPN like in the pure P(VDF-TrFE) samples. On the other hand the area, that is covered with 4CzIPN, still shows partial filling of the pores, like it was seen for PFO. When a porous film, which had pores with larger diameter due to an uncertainty in the production, also showed larger pores in the 4CzIPN covered areas, it was proofed that those are the insufficiently filled pores underneath. For areas covered with 4CzIPN the depth of the pores in this film compared to the surrounding 4CzIPN add layer was measured. This and all other data on the spin-coated samples can be found in table B.3.
Initially it was unsuccessfully attempted to create an even 4CzIPN layer with properly filled pores and a not to large add layer by changing the solution concentration and the spin-coating speed. Afterwards new attempts were made with the surfaces of the porous films being treated prior to the deposition of the 4CzIPN to improve the attachment of the semiconductor solution and create even films. UV/ozone, oxygen plasma and nitrogen plasma were used, but only the oxygen plasma was successful. An image of that sample can be seen in figure 4.10 (c). When the performance of that device was measured, it didn't show a correct hysteresis curve, but too high current for low voltages, similar to the PFO samples with insufficiently filled pores. The increase in photocurrent was insignificant.
Apart from the variations in spin-coating, it was also attempted to fill the pores in the ferroelectric polymer by bar-coating the 4CzIPN solution. Table 4.3 shows the results of the bar-coating and in figure 4.10 (d) the rough surface produced by this method can be seen. The measurements of the film thickness revealed that it varied strongly across the device areas and the performance could not be improved compared to the spin-coated samples.

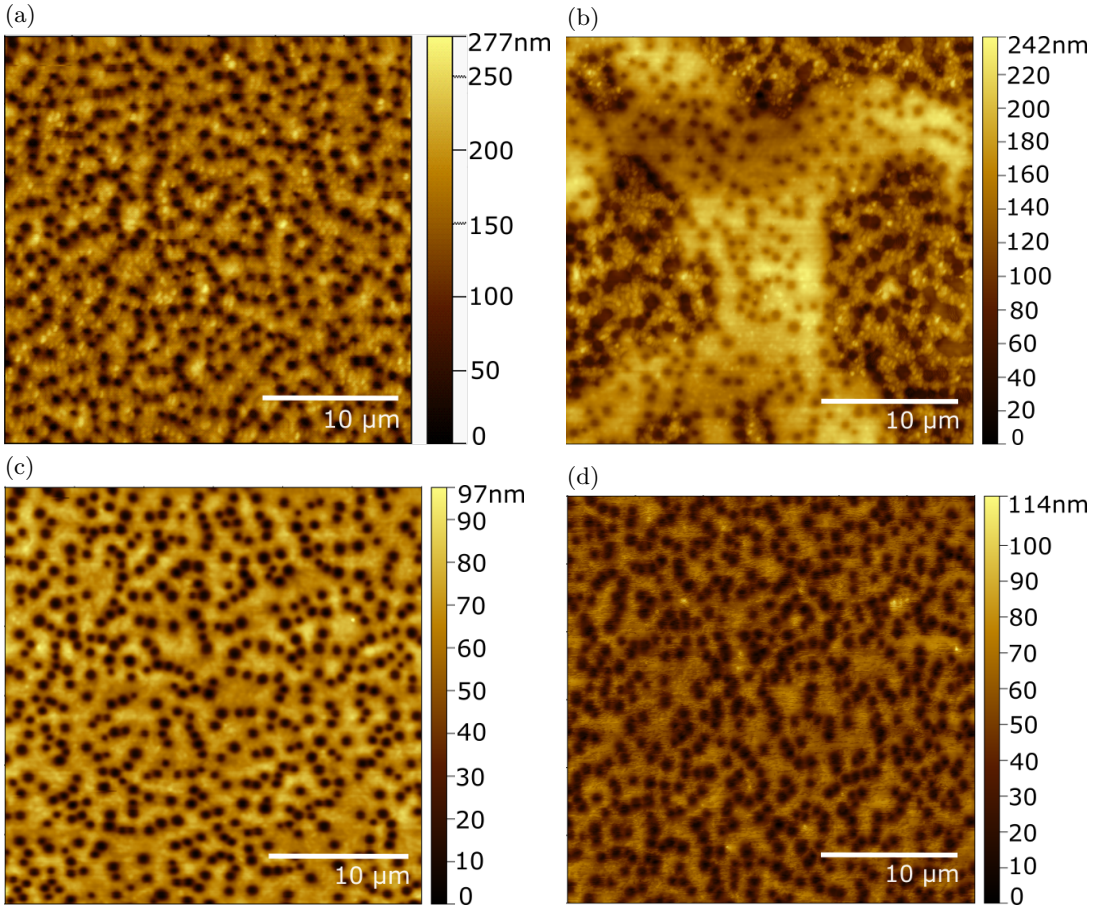

Figure 4.10.: Images of devices backfilled with 4CzIPN as the semiconductor. Figure **(a)** shows the porous P(VDF-TrFE) film before any 4CzIPN was added, **(b)** is sample 5 in table B.3 and is an example for how the uneven coverage with 4CzIPN looked. In **(c)** sample 7 from B.3 is seen with a continuous layer of 4CzIPN partially filling the pores and as the add layer on P(VDF-TrFE). Finally **(d)** is a sample produced with bar-coating technique.

	solution volume deposited [ul]	temp. heat plate [°C]	pore depth in TADF film [nm]	add layer thickness [nm]
1	100	50	25 to 35	90 to 100
2	50	40	40 to 50	25 to 35
3	100	40	50 to 60	20 to 30

Table 4.3.

4.2. Multilevel switching of P(VDF-TrFE):PFO blend film devices for use in neuromorphic applications

For the following measurements P(VDF-TrFE):PFO devices produced by the common blend film method as described in section 3.2.3 were used. The chosen mask for the electrodes produced 25 devices per sample.

4.2.1. Initial characterisation

The quality of the fabricated samples was controlled by testing each of the 25 electrode cross-sections (named A1 through A25). All the measurements were performed with the samples in a vacuum chamber and the voltage was applied and the current measured with a Keithley 4200-SCS. For this measurement the voltage was slowly increased from 0 V to 26 V, then lowered to −26 V and increased again to 0 V. In figure 4.11 the positive side of the sweep, showing the characteristic hysteresis of the ferroelectric material, can be observed. The high majority of the devices was functioning and showed very equal performance throughout the device in the I-V sweep measurement. This enables one to use different devices on the sample for a variety of measurements without the need to characterise each of them individually.

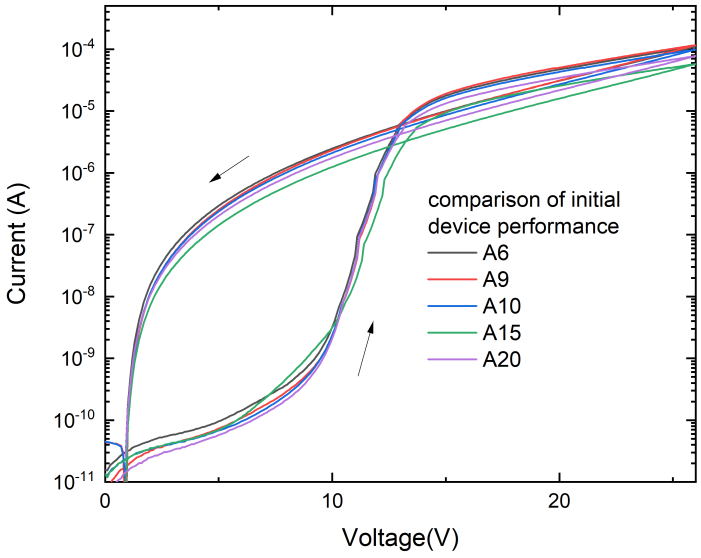

Figure 4.11.: Hysteresis measurements of different devices spread over the whole sample area showed very comparable performance results.

With the increase in applied voltage above a certain voltage level (around 10 V) a clear increase in current output can be observed. This indicates the switching of the polari-

sation of the dipoles in the ferroelectric polymer domains of the blend film. Upon the downward voltage sweep from the maximum value to 0 V the polarisation is remnant and therefore a clear hysteresis can be observed. For the following measurement 5 V was chosen as the read-out voltage. The minimal current value measured for a sample of full polarisation in the direction opposite the applied electric field will be referred to as the minimum current state or OFF state of the device. The maximum current state or ON state is found for the ferroelectric polymer being fully polarised in the direction of the field vector. Figure 4.11 shows that at 5 V the ratio between the ON state current and the OFF state current for the slow sweeping measurement exceeds 10^3 in all devices.

4.2.2. Application of voltage pulses to address and read multilevel polarisation states of P(VDF-TrFE)

4.2.2.1. Measurement with the Keithley 4200-SCS

The initial task involved the finding of the ideal measurement set-up to address and read out the polarisation state of the blend film device. The idea was to utilise a pulse train comprised of reset, write and read pulses. The reset pulse of −20 V and sufficient pulse width was used to bring the device in the fully depolarised state (dipoles oriented antiparallel to the field direction of the write pulse). This way a dependence of the resulting polarisation state on the previous one could be excluded. The write pulses were applied to set a certain polarisation state and read pulses of 5 V were meant to determine the current polarisation. Figure 4.12 depicts a schematic of a pulse train.

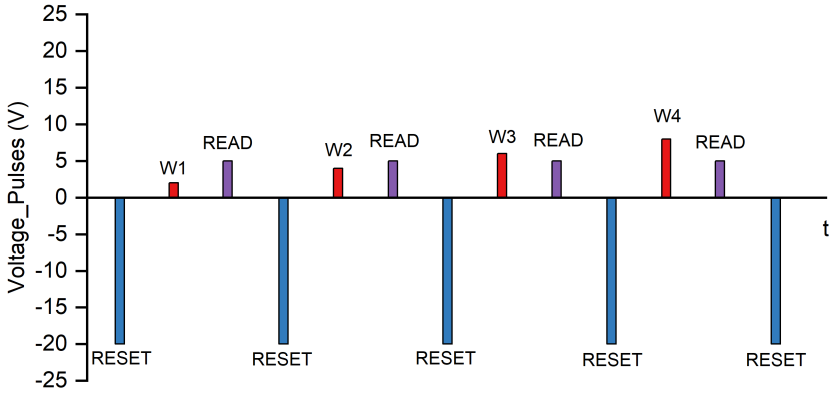

Figure 4.12.: The schematic shows a pulse train consisting of reset, write and read pulses as it was used to address and read-out polarisation states of the P(VDF-TrFE):PFO diode.

While the Keithley is capable to apply the pulses correctly, the current output that

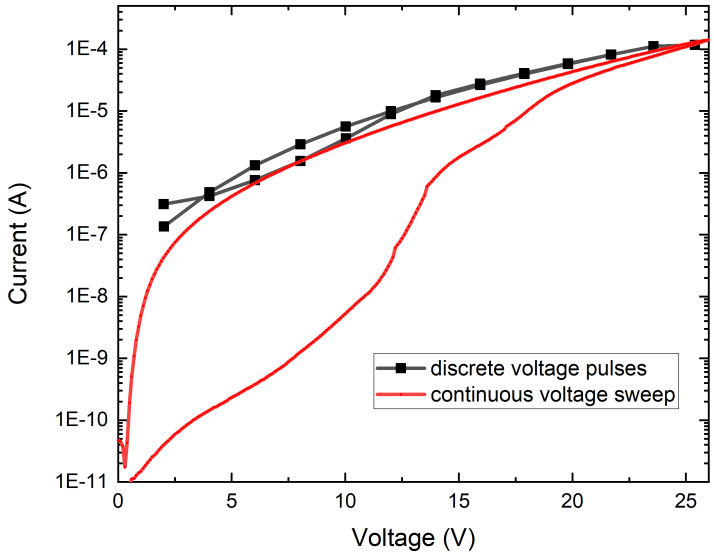

Figure 4.13.: Comparison of the results of applying voltage pulses or a continuously increasing voltage to the blend film device. These measurements were conducted with a Keithley 4200-SCS and the current measured for the pulses was incorrectly high due to device limitations.

was measured by the PMU was too high for the OFF state (see figure 4.13). The measurement with the PMU allows for high time resolution (compare figure 4.14), which shows charging and discharging in the device. On the other hand the experiments also demonstrated that the current values could not be measured correctly as the precision of the PMU could only resolve currents at a µA scale, while a 1×10^{-12} A resolution was needed for the correct measurement. The Keithley was able to measure the continuously increasing voltage sweep, because this measurement uses the SMU, which has the right precision, but less time resolution. Therefore it is suitable for the slow sweep, but not the fast pulsing.

4.2.2.2. Measurement with high resolution oscilloscope and preamplifier

In order to determine the current levels of the pulsed measurement correctly an external measurement with high time resolution and high current resolution was needed. To achieve both a combination of a current preamplifier and an oscilloscope with high sampling rate was used. The pulses were still applied with the Keithley 4200-SCS.
During testing of the new measurement set up, several issues became apparent. It was attempted to increases the current levels from OFF to ON state level by applying a pulse train like it is shown in figure 4.12 and increase the amplitude with every write pulse to increase polarisation along the field vector. Generally this type of experiment

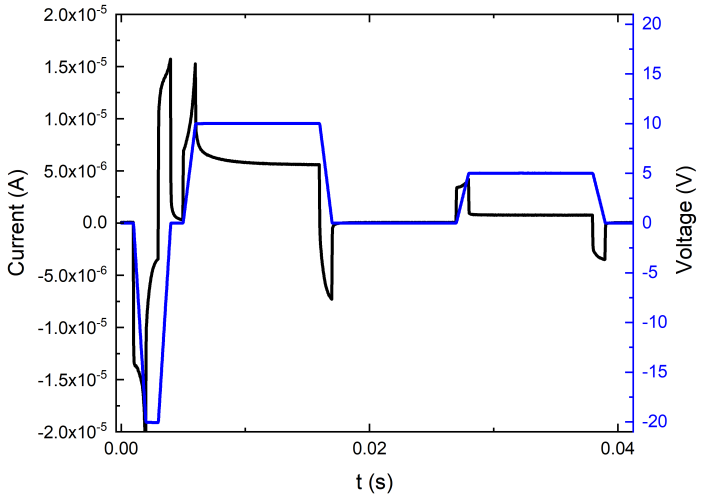

Figure 4.14.: Result of simultaneously applying voltage pulses and reading current with the Keithley 4200-SCS. The time resolution was precise enough to observe charging and discharging in the device, but the current values cannot be taken as correct due to limitations of the measurement with the PMU.

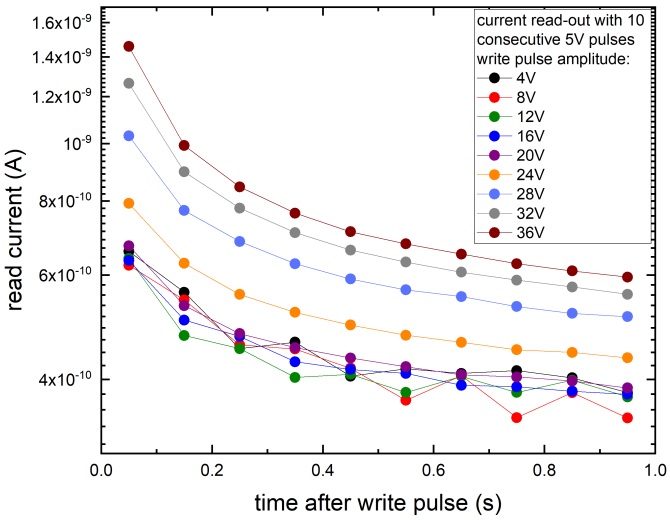

Figure 4.15.: Ten consecutive 5 V read pulses were applied to the device after a write pulse. It can be seen that a stable value wasn't reached yet 1 s after the write pulse. The read pulse width was 50 ms.

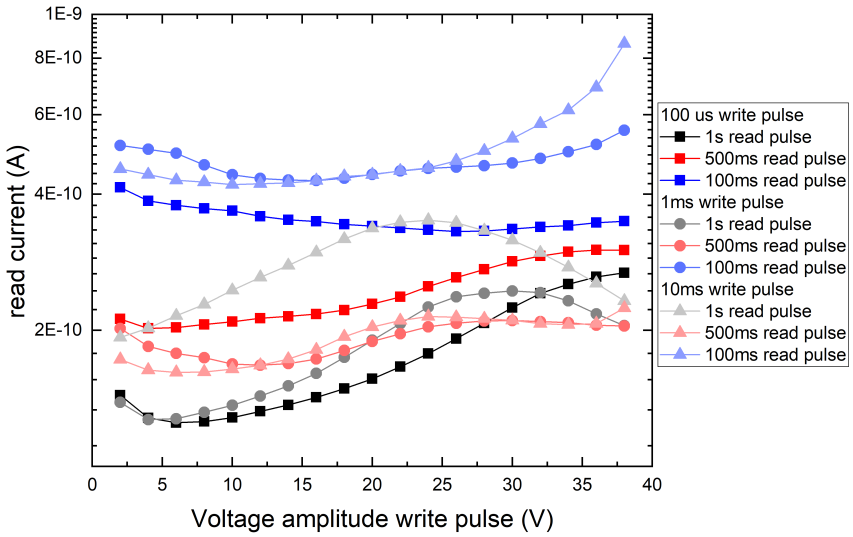

Figure 4.16.: Dependence of the read current level on write and read current width for measurement of the pulse train with the preamplified signal with a high resolution oscilloscope.

could never show a large increase in current, which was later explained with fatigue (compare 4.2.4). The variation of the timing in the pulse train would additionally show complications with the pulsed read out. In figure 4.15 one can see the result of applying ten consecutive read pulses (5 V, 50 ms) after each write pulse. While the current value shows some increase with increasing amplitude, the difference is below expectation. It also becomes evident that the polarisation state of the device takes time to stabilize as the read-out current still decreases 1 s after the write pulse.
A similar observation could also be made, when the read pulse width was increased. In figure 4.16 can be observed how shorter read pulses of 100 ms (blue) showed again higher current levels like for the early pulses in figure 4.15. An increase in read current due to increasing amplitude can also not be observed. For a long read pulse of 1 s (black) the expected switching starts to show. With the long read pulse one can begin to observe that increasing write pulse width will also effect the switching behaviour. For a longer write pulse lower voltage amplitudes are necessary to reach the same polarisation state.
In order to determine whether it was due to write pulses or the pulsed read-out that only a small increase in current could be observed, the test shown in figure 4.17 was conducted. When the SMU of the Keithley 4200-SCS was used to read the current level with a slow sweep between 0 V and 5 V the expected result for the OFF state could clearly be reproduced after a depolarising pulse was applied. When a polarising pulse

was used to switch the device into the high current ON state, the expected read current values could also be reproduced by sweeping from 5 V to 0 V. This demonstrates that the addressing with pulses is able to put the device in the desired state. The issue therefore must be with the pulse train, which includes a pulsed read-out.

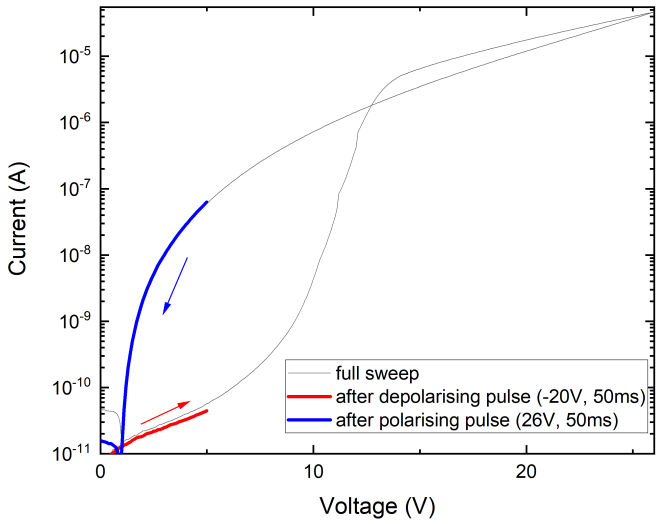

Figure 4.17.: A voltage sweep from 0 V to 5 V after a depolarizing pulse of −20 V and a sweep from 5 V to 0 V after a polarising pulse of 26 V shows that the write pulses can bring the device into the desired polarisation state.

4.2.3. Switching of the polarisation state with variation of amplitude and width of the write pulse

Since the voltage sweep from 0 V to 5 V with the SMU of the Keithley 4200-SCS is a proper way to read the current level, this was applied for the following measurements. The focus was put on the write pulses allowing to facilitate the multilevel switching, rather than the problematic read-out with pulses. Figure 4.18 as an example depicts that the write pulses are able to switch the polarisation state with several intermediate states.

By applying write pulses with increasing amplitude, it can be seen that the coercive field initializing the switching of dipoles is dependent on the pulse width (compare figure 4.19). For longer pulses a lower voltage amplitude is sufficient. It can clearly be observed that independent of the chosen pulse width the same minimum and maximum current levels can be reached. Besides this it is shown that for longer pulse width the switching takes place faster with less intermediate steps compared to a short pulse.

On the other hand a very similar switching behaviour can be observed, when the write pulse amplitude is fixed, but the pulse width increased. As expected for lower ampli-

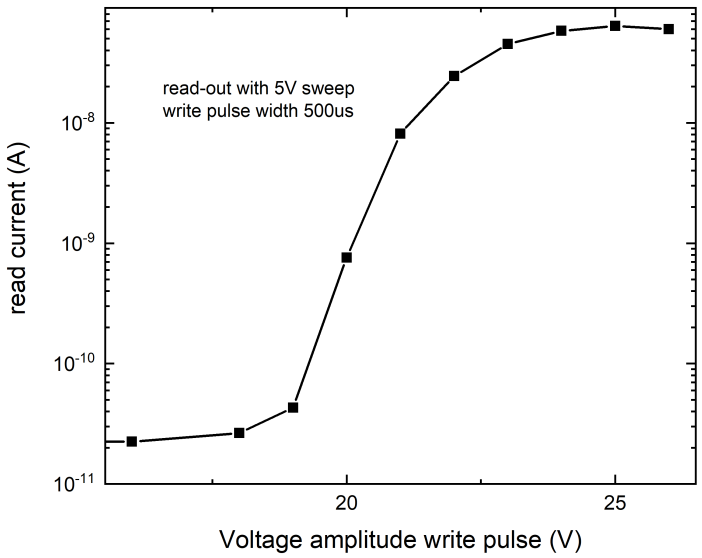

Figure 4.18.: Example for switching the device from the low current OFF state to the high current ON state by application of write pulses with increasing amplitude.

tudes longer pulse width is necessary to address certain polarisation states (compare figure 4.20).
Figure 4.21 depicts how in the same way the device could be brought from the high current to the low current state by applying all the pulses with inverted sign. First a (20 V, 50 ms) positive reset pulse was applied to put the device in the ON state and then write pulses with increasingly negative amplitude were applied to switch the polarisation. When plotting the read-out current dependent on the absolute voltage amplitude, it is possible to compare the two switching types easily. It can be observed that the initial ON state for switching from ON to OFF state is less stable than the OFF state and already decreases, before pulses above the coercive field are applied. For the actual switching behaviour the two processes show the exact inverted response to the write pulses. Therefore all polarisation states can be addressed predictably.

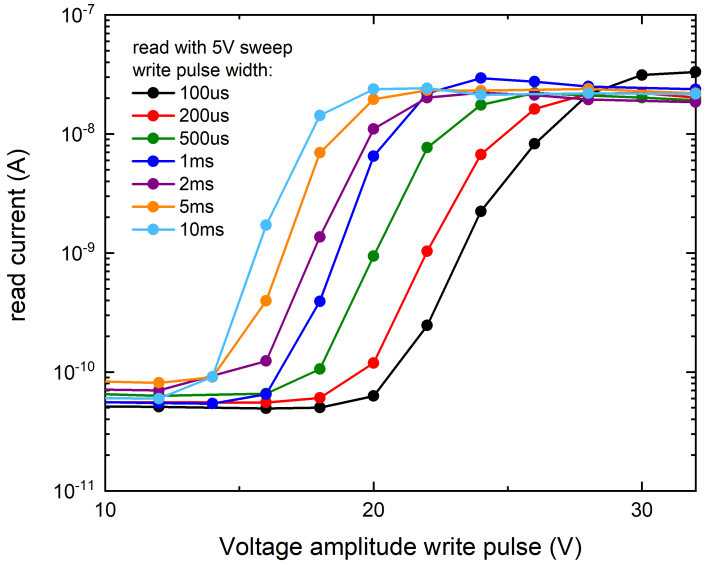

Figure 4.19.: Switching the polarisation state of the P(VDF-TrFE):PFO device by applying write pulses with increasing voltage amplitude.

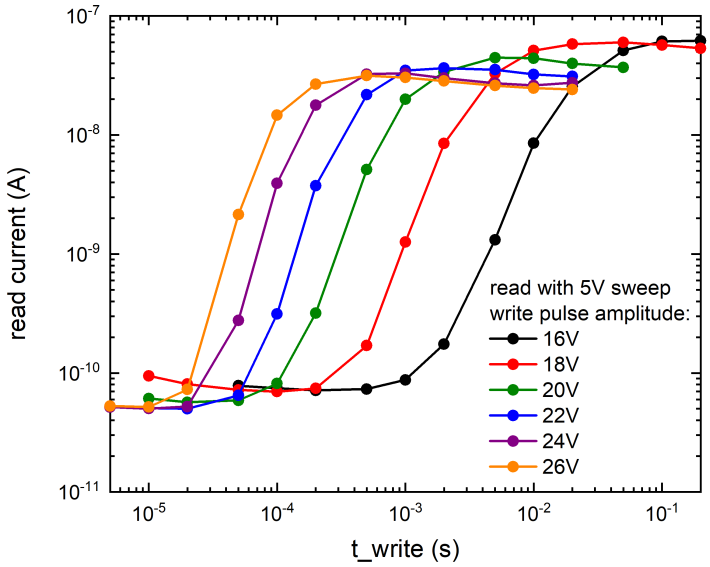

Figure 4.20.: Multilevel switching observed for pulsing with increasing pulse width.

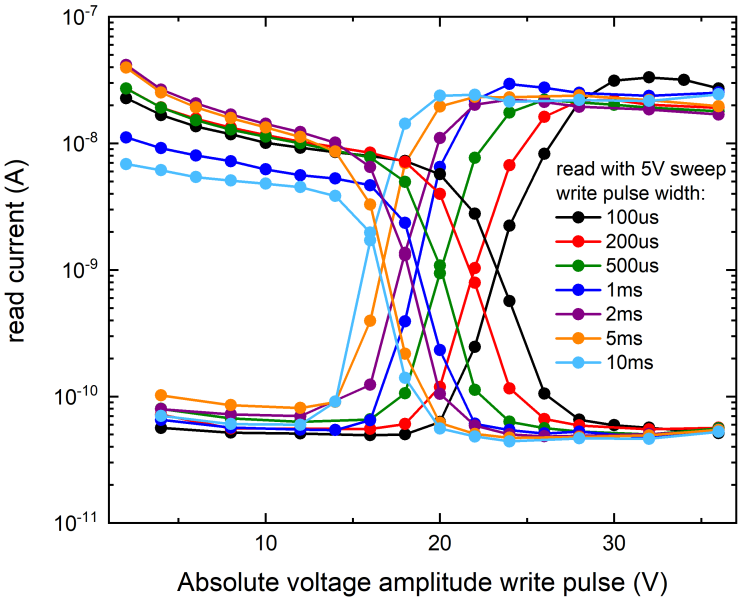

Figure 4.21.: Polarisation switching observed for both switching from OFF to ON state with write pulses of positive polarity and from ON to OFF for write pulses with negative polarity.

4.2.4. Stability of the multilevel polarisation states – retention time and fatigue issues

In order to determine the stability of the polarisation states over time, each states was addressed with a write pulse of a certain amplitude and then read-out at specific delays after the write pulse. In figure 4.22 one can see the dependence on time delay. Between OFF and ON state six clearly distinguishable intermediate states were addressed. Even after a delay time of 1500 s all states were still very close to the read current of the initial measurement and easily differentiable from each other. The stability of the intermediate states was not any less than for the minimum and maximum state. The ON state again showed some instability.

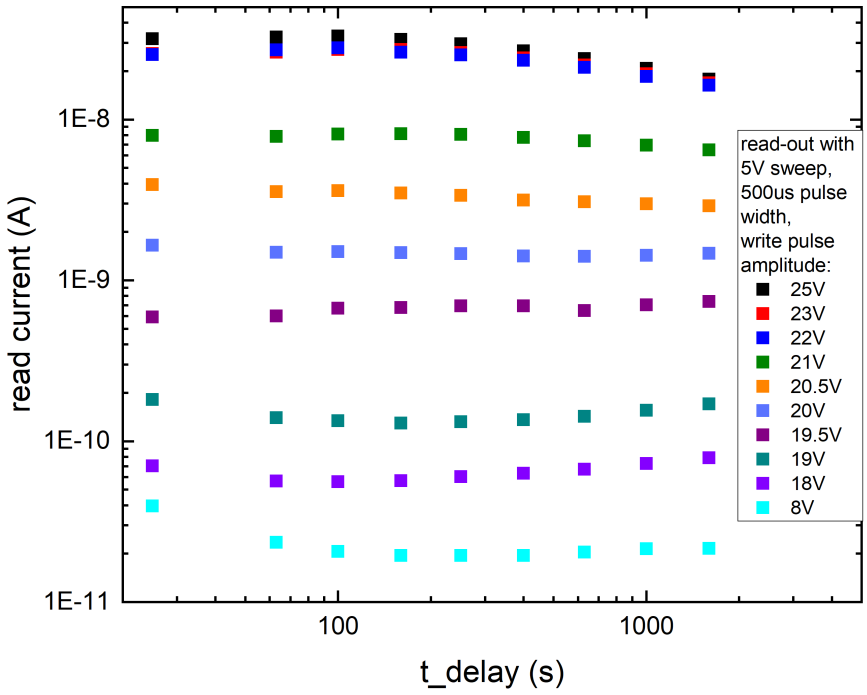

Figure 4.22.: Retention time measurements for the OFF and ON state, as well as several intermediate states. The intermediate polarisation states show good stability over time.

When conducting several measurements on one device during the course of one day (or even more strongly for reusing the device on another day) a fatigue of the device performance can be observed. The comparison of the I-V sweeps already shows a decrease in maximum current values reached and ON/OFF ratio at 5 V (see figure 4.23), but the pulsed measurements are even more strongly affected. Still the swept measurement demonstrates that the fatigue already starts to show after just one measurement.
When comparing the pulsing of a fresh device and a fatigued one, large differences can be seen. Figure 4.24 shows the strong decrease in the ON state current value for the fatigued device and also the increase of coercive field for the same pulse width. The measurement with pulses of fixed amplitude and increasing pulse width (figure 4.25) is also significantly affected by fatigue. For lower amplitudes the maximum current value that can be reached decreases and even doesn't exceed a certain current level at all anymore, when the amplitude is low. This can't even be overcome by going to really long pulses width (up to 1 s).

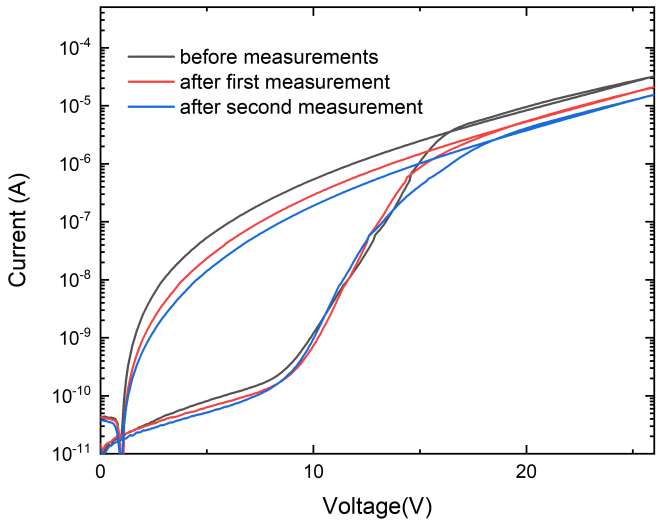

Figure 4.23.: Each measurement will fatigue the device. This is observable in the I-V curve.

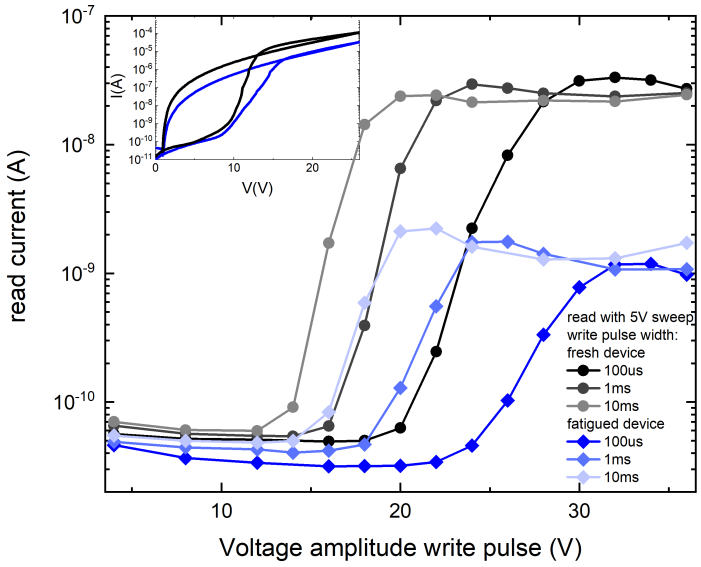

Figure 4.24.: Fatigue has a strong effect on the maximum current that can be reached for the ON state of the P(VDF-TrFE):PFO device and the voltage amplitudes necessary for switching to higher values increase

Therefore it became clear that the pulsed measurements with the P(VDF-TrFE):PFO blend devices were only reliable on fresh devices and had to be changed, when they showed fatigue.

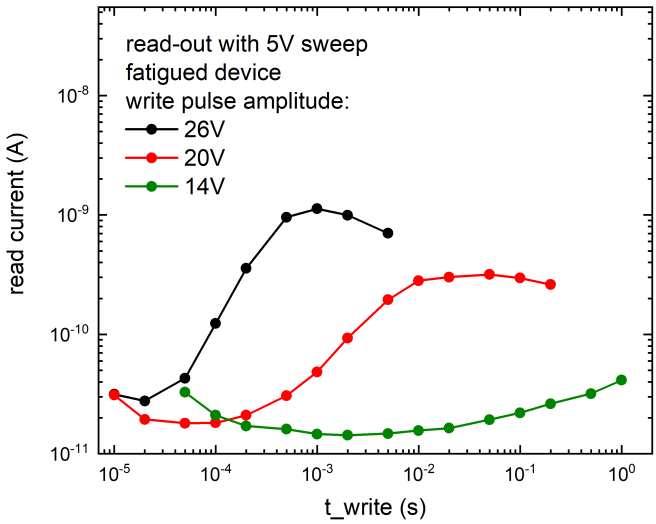

Figure 4.25.: For a fatigued blend film device the maximum current value will depend on the applied write pulses amplitude. With decreasing amplitude the maximum current doesn't exceed a certain level, even if much longer pulses are applied. This isn't the case for fresh devices (see figure 4.20).

4.2.5. Switching of the polarisation state with increasing number of repetitions of the write pulse

The aim was to show that a stepwise switching could also be achieved by applying write pulses with parameters below the coercive field repeatedly with increasing number of repetitions. The OFF and ON state current values for the previous measurements with increasing amplitude or width were taken as reference.
Initially a reset pulse (−20 V, 50 ms) was applied, then a certain amount N of pulses and thereafter a read-out with the sweep to 5 V. The expectation was to see an increase in current dependent on the number of write pulses. Variations were made for the amplitude of the write pulses, the frequency of pulses and the waiting time between individual pulses to see how they can influence the current levels measured.

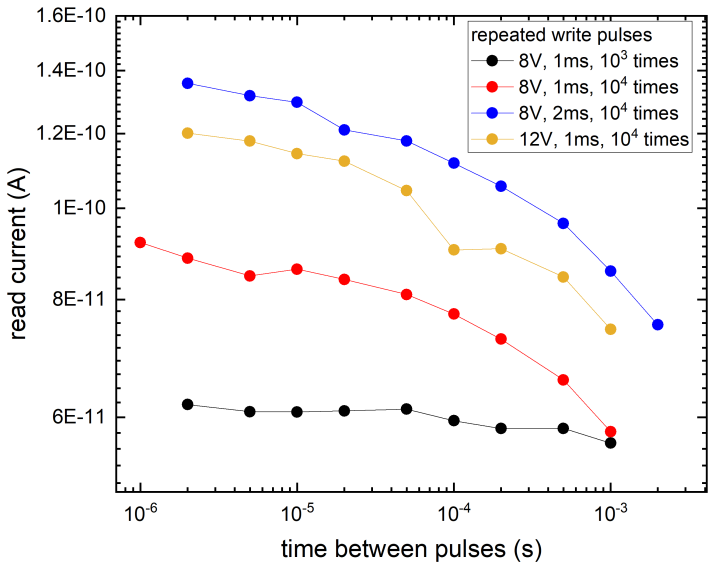

Figure 4.26.: For repeated application of identical write pulses the variation of the time between pulses could only show a small increase for smaller pauses. No significant increase in read current was observed.

For the first measurements the amplitude of the write pulses was kept below the coercive field to ensure that the device wasn't changing its polarisation due to an individual pulse, but rather the repetition. The first idea was to keep the length of time t_{on}, that the individual write pulse was applied, identical with the pause between pulses t_{off}, so only the frequency was changed. Variation of the pulse amplitude (4 V, 8 V, 12 V) and pulse width (10 ms, 5 ms, 2 ms, 1 ms, 500 µs, 200 µs, 100 µs, 50 µs, 20 µs, 10 µs) were tried. For most no difference in read current could be observed, when increasing the number of pulses N. Some showed a small increase, but only within one order of magnitude. The second idea was to keep t_{on} always same and decrease the

length of the pause between pulses t_{off}. This could have an effect, if the problem is that the small amount of polarisation switching, that was achieved by an individual pulse, relaxes again during the break. So for this the read current would increase with the break between pulses decreasing. In figure 4.26 can be observed the decrease in t_{off} (from 1 ms to 2 µs) could only show a small increase in read current.
Next it was attempted to reach full polarisation switching with repeated pulses by using longer pulses width. Pulsing with a 50:50 duty cycle (t_{on} and t_{off} identical) did not show any significant increase in current even for pulses of up to 50 ms duration (amplitude 12 V). When the amplitude was increased to 14 V, already close to the coercive field, and t_{off} was decreased to a thousandth of t_{on} (e.g. 2 ms on, 2 µs off) an increase with amplitude (compared to the measurements with 12 V) and an increase with pulse width was observed, as it can be expected from the previous measurements (see figure 4.27). An increase with number of pulses N of about one order of magnitude was shown.

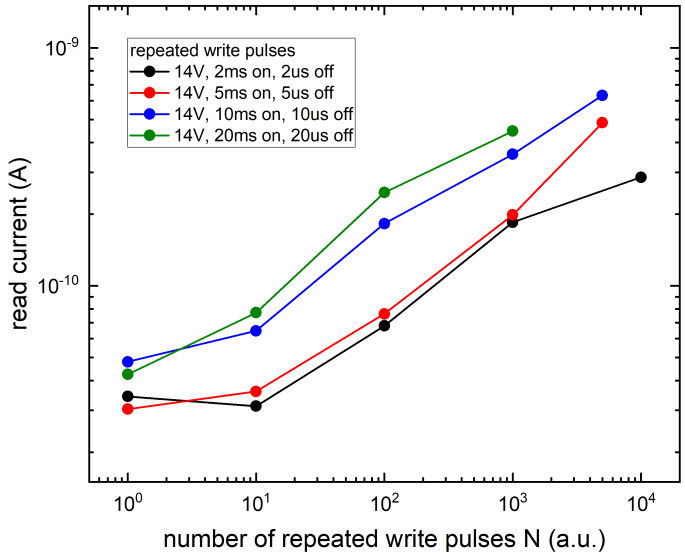

Figure 4.27.: For a pulse amplitude of 14 V (close to the coercive field) an long pulse width an increase in read current with the number of applied pulses could be observed.

It was noticed that these measurements with repeated pulses showed a strongly fatigued the device. Therefore the currently reachable ON state current level was determined before and after each measurement by applying a pulse (25 V, 500 µs) known to switch the device to the full ON state followed by a read-out. This was done to ensure that the lower increase in read current seen in figure 4.27, compared to the measurements with increasing pulse amplitude and width, was not due to fatigue of the device. The ON state levels indicated in figure 4.28 and 4.29 show the strong

fatigue effect of the measurements and proof that even the lowered ON state was not reached. The device had been fresh before the measurements shown in figure 4.28.
It was now attempted to switch the polarisation of the device by using repeated pulses with high amplitude above the coercive field and shorter pulse width (opposite to the earlier attempts with low amplitude and long pulse duration). Figure 4.28 shows that even for a amplitude of 18 V and 19 V the ON state could not be reached. It was also attempted to reduce fatigue by having longer t_{off}, but the ON state level after the measurement was still strongly reduced.

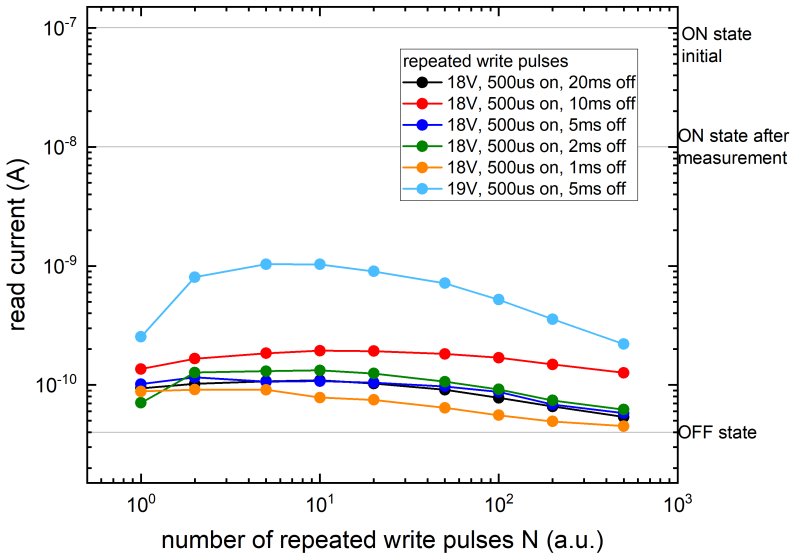

Figure 4.28.: In order to avoid fatigue of the device longer off time between pulses and higher amplitudes were used. It can be seen that the ON state level was still strongly reduced after the measurement, while the polarisation could not be switched.

Further measurements with very high amplitude of 25 V and shorter pulse duration (figure 4.29) show how the current increases with pulse length (which has already been shown in the measurement with increasing pulse width) to almost the ON state level. This can again not show the intended increase from OFF to ON state current level with increasing number of pulses, since applying a single pulse already brings the device into an elevated polarisation state. For 100 µs pulse width there is some increase from a lower to a higher intermediate state (but not switching from OFF to ON state), so this also doesn't give the desired result.
These measurements show a strong fatigue effect of applying pulse trains to the device. This brings up the reasonable suspicion that the failure to show a strong increase in current for the earlier measurements with a pulse train of reset, write and read pulses (section 4.2.2) was also effected by fatigue.

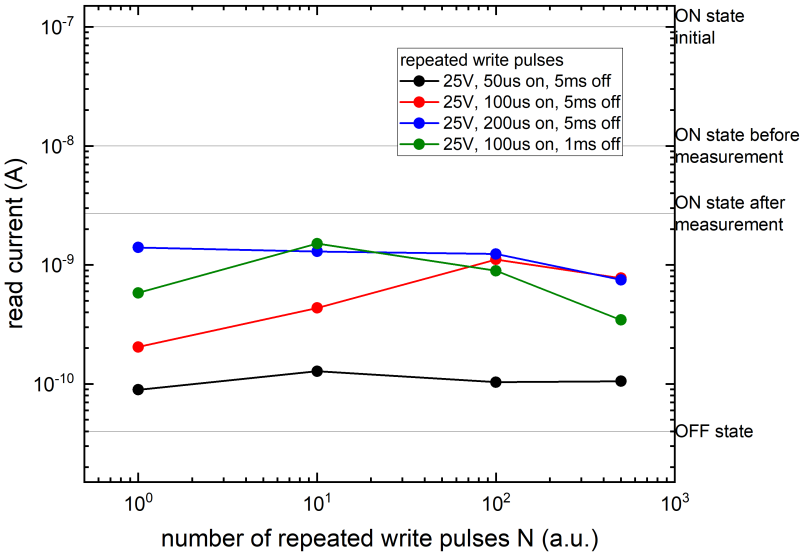

Figure 4.29.: Pulsing repeatedly with high amplitude shows the expected increase with pulse width, but can also not bring the intended increase from OFF to ON state with increasing repetition number N. Fatigue of the ON state can again be observed.

4.2.6. Application of pre-spike and post-spike pulses to emulate synaptic behaviour

In the previous chapters was shown how the P(VDF-TrFE):PFO blend film device responds to the application of voltage pulses to one electrode, while the other electrode is kept grounded. In the biological synapse, whose behaviour we intend to simulate in order to go towards the goal of neuromorphic computing, the state of the synapse called synaptic weight is defined by the timing of two electric pulses reaching the neuron (compare 2.7). Therefore we need to apply pre-spike and post-spike pulses to indicate spike timing dependent plasticity (STDP).
First the response of the device to the application of two simultaneous pulses at the top and bottom electrode is observed. The polarisation state, that will be reached, therefore dependents on the difference between the voltage levels at the two electrodes and the timing. For the measurements in figure 4.30 the two pulses were kept at the same pulse width (500 µs) and matched up exactly in timing. While one electrode was always supplied with a -10V pulse, named as the post-spike pulse, the pre-spike pulse applied to the other electrode increased in amplitude. When comparing figure 4.30 to figure 4.19 (pulsing with increasing amplitude at just one electrode) a very similar switching behaviour can be seen. The pre-spike pulse amplitudes needed to address a certain polarisation state are shifted by around $-10\,\mathrm{V}$ as expected, so that the device is clearly effected by the total difference in voltage potential across both electrodes.

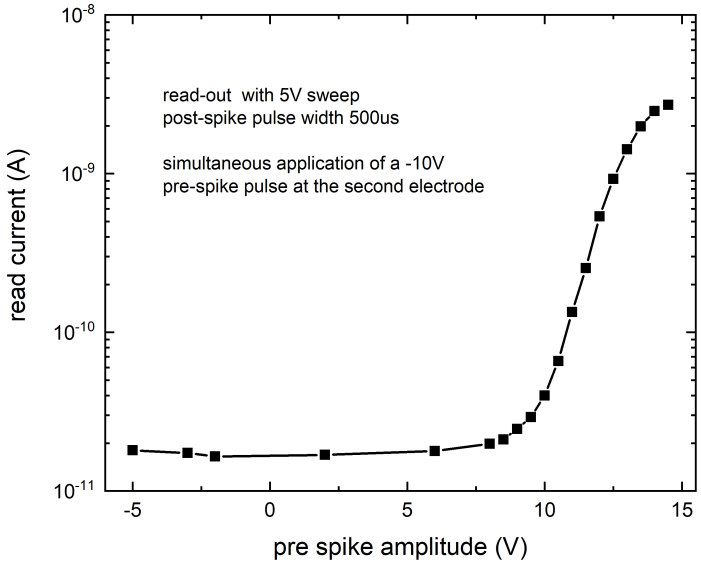

Figure 4.30.: Addressing the blend film device by applying voltage pulses to both electrodes simultaneously, so that the polarisation state dependents on the total voltage difference.

To simulate the timing dependency of the synapse, with depression for the post-spike pulse being before the pre-spike pulse and potentiation for the opposite case (compare figure 2.9 in chapter 2.7), the strategy shown in [36] is used. The pre-spike pulse is applied as the pulse train shown in the lower image of 4.31, so that the amplitude of each individual pulse is below the coercive field. The timing of the the post-spike pulse ($-10\,\mathrm{V}$, $500\,\mu\mathrm{s}$) is chosen to line up exactly with the timing of one of the pre-spike pulses. Therefore the total potential will be above the coercive field and the polarisation state will be changed accordingly. By chosing the pre-spike pulse amplitudes as shown in 4.31 the polarisation state of the blend film device dependents on the timing of the post-spike pulse in the same way as the synaptic weight. For the post pulse being slightly earlier than the as 0 labeled point in time there will be maximum depression and equally for potentiation.

4.2.7. Addressing and read-out of individual P(VDF-TrFE):PFO blend film devices in a 2x2 array

After the multilevel switching in a P(VDF-TrFE):PFO blend film device has been extensively analysed, the focus was now put on a 2x2 array of four such devices as a first step of up-scaling. Chapter 3.5 explains, how individual devices were addressed with a switching board and the potential applied to each line in the array was controlled. These measurements were conducted with a different sample than the

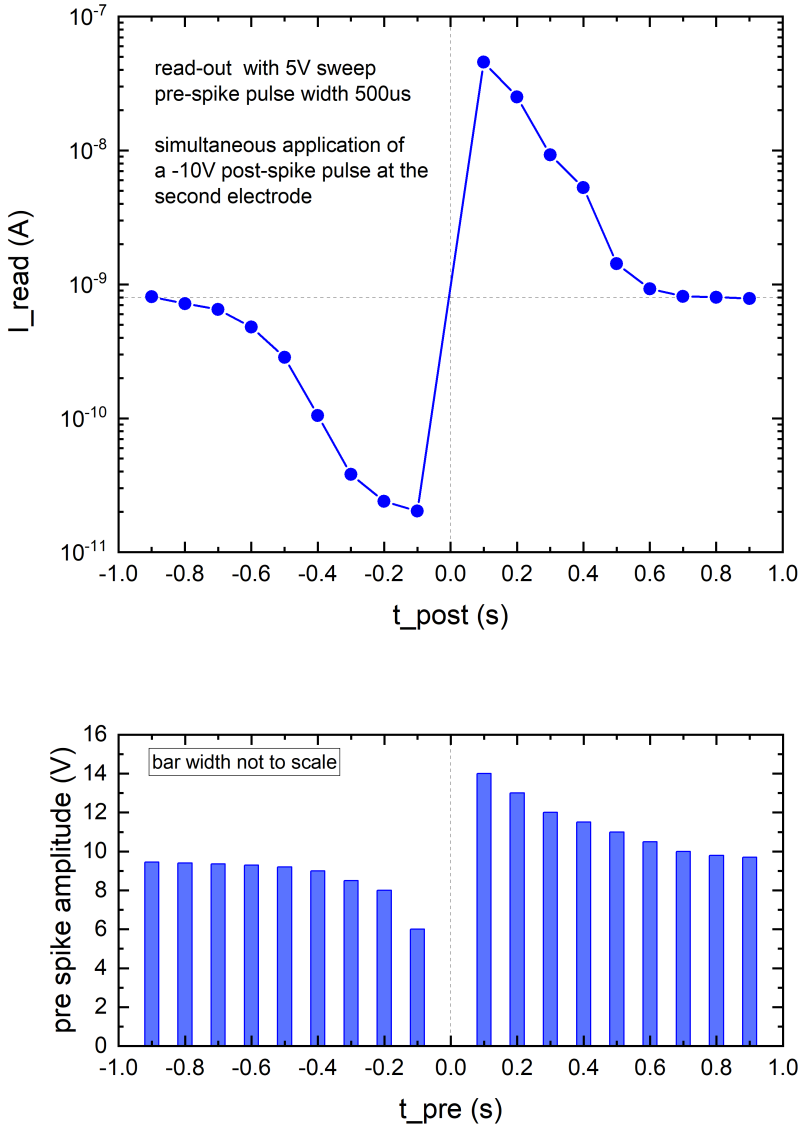

Figure 4.31.: The pre-spike pulse train is shown in the lower image. The post-spike pulse is always chosen, so that it is applied simultaneously with one of the pre-spike pulses. In this way timing dependency and by chosing the pulse amplitudes deliberately depression and potentiation can be shown.

previous ones, which had been processed from the same solution, but spin-coated with a lower speed. Therefore the film thickness was higher ((211.8 ± 16.3) nm compared to (258.8 ± 5.3) nm) and the pulse amplitudes needed were shifted about 4 V higher than before. For the measurements the pre-spike pulses were applied to the active word line and the post-spike pulses to the active bit line, while the inactive lines were kept grounded.

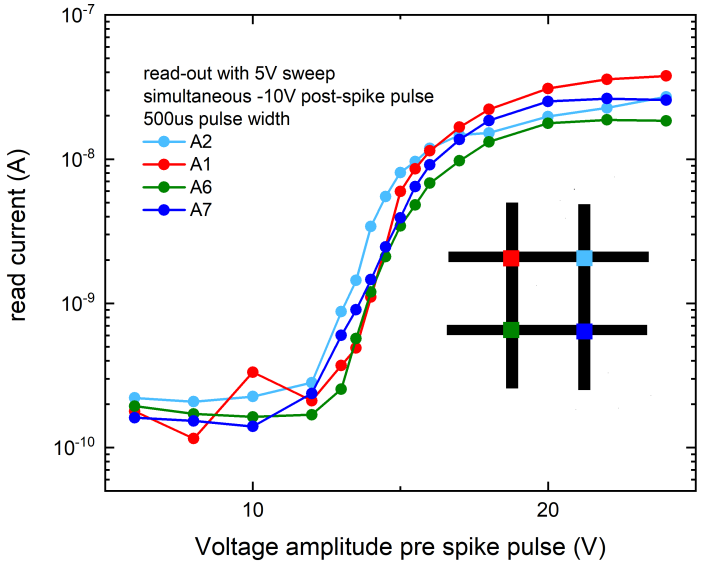

Figure 4.32.: Switching of the polarisation state of four P(VDF-TrFE):PFO blend film devices in a 2x2 array.

All devices were switched from the OFF to the ON state and read-out one after the other. Figure 4.32 shows that all parts of the array show very similar switching characteristics with comparable coercive field and ON state values. Therefore the set-up allows for reliable addressing of each device.
In order to test the 2x2 array of P(VDF-TrFE):PFO blend film devices for cross-talk between the devices, indicated by the polarisation state of a neighbouring device being changed, test measurements were conducted (compare 4.33). The inset in figure 4.33 (a) shows the order in the array. These measurements had been conducted on a different array than those of figure 4.32 due to the first array being affected by fatigue. The polarisation state of each device was measured before (black squares) and after (red squares) pulses were applied to device A12. The inactive lines were kept grounded. For measurement (a) all devices were brought to the OFF state, then -10 V post-spike pulses were applied to B2 and pre-spike pulses with increasing amplitude to W1 to switch A12. It can be seen that the polarisation state of device A11 was greatly varied. The suspicion was that the polarisation was changed, because this device felt

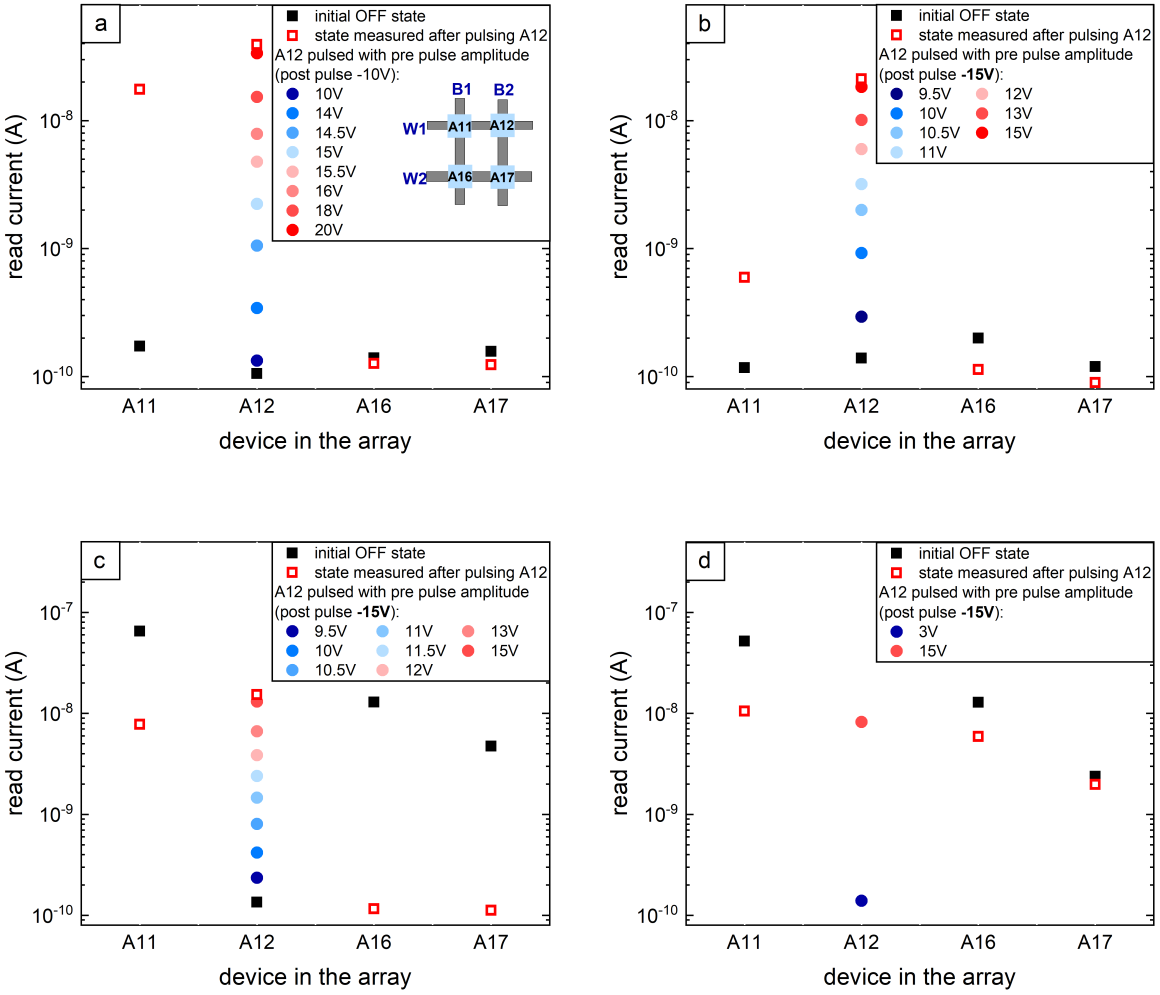

Figure 4.33.: Testing the 2x2 array of P(VDF-TrFE):PFO blend film devices for cross-talk. The inset in (a) shows the order in the array. The polarisation state of each device was measured before (black squares) and after (red squares) pulses were applied to device A12. The inactive lines were kept grounded. **(a)** initially all devices in OFF state, then A12 was switched to ON state; (b) same as (a), but larger post-spike pulse amplitude was applied; **(c)** initially all devices in ON state, A12 was switched from OFF to ON state; **(d)** same as (c), but only one pulse to the OFF state and one to the ON state were applied to A12.

the potential between B1 being grounded and pre-spike pulses of up to 20V being applied to W1. Therefore for measurement (b) all devices were brought to the OFF state again and then A12 was switched by applying higher post-spike pulses of $-15\,\mathrm{V}$ to B2. The pre-spike pulses on W1 were then lower in amplitude than in (a) and the polarisation state of A11 was much less effected. For the following measurements the post-spike amplitude was kept at $-15\,\mathrm{V}$. For (c) all devices were switched ON and it can be observed that the ON state level of each device varied significantly. Initially it was suspected that this was due to variation in thickness in this area , but measurements proofed this wrong (compare table B.4). It is a possibility that the two polymer materials were not well distributed in this area or domains had formed unevenly in the area of the second array used for the measurements in figure 4.33. A12 was switched from OFF to ON state, which effected the polarisation state in the other devices strongly. A16 and A17 were even brought to the OFF state. In (d) the previous measurement was repeated, but only one pulse to the OFF state and one to the ON state were applied to A12. The effect on the neighbouring devices was smaller, but still visible. The OFF state had already looked less stable in the retention time measurement (figure 4.22) and the fatigue measurements (figure 4.24 and 4.25) than the OFF state, so it is unsurprising that it is also more strongly affected by cross-talk.

4.2.8. Observations for addressing the polarisation states in the P(VDF-TrFE):PFO blend device with voltage pulses

A detailed measurement of the multilevel switching behaviour of the P(VDF-TrFE):PFO blend device is shown in figure 4.34. In (1) the voltage amplitude was increased in $+0.5\,\mathrm{V}$ steps and afterwards in (2) the device was brought to the OFF state again by pulsing with decreasing -0.5 V steps of increasingly negative pulses. This shows several features, that have been observed in the other measurements as well.

For one it can be seen that the ON state current level, reached with the highest positive amplitude pulse at the end of (1), immediately decreases significantly upon the first negative voltage pulse. A similar "instability" of the ON state was seen in figure 4.21 and the retention time measurement figure 4.22 already. It can also be observed that the decrease in (2) is slower than the increase in (1) and also not the same OFF state level was reached. The very slow pulsing experiment with even smaller step size than seen in the figure (as small as $+0.1\,\mathrm{V}$ and -0.1 V), which overall took more than two hours, showed a certain memory effect, since the same low current level wasn't reached again. This was not observed for fast switching (figure 4.21).

Other measurements also showed a time-scale and timing dependency. In chapter 4.2.2 the read pulses showed different result for varying the timing and duration of the read pulse and only a slow swept read-out gave reliable results. A different observation, which was made throughout the pulsed-addressing measurements in the chapters above, is plotted in figure 4.35. It was observed that the ON state current level, that was reached in the slow voltage sweep was never reached with voltage pulses. The OFF state current was equal or slightly higher for pulsing. Therefore the ON/OFF

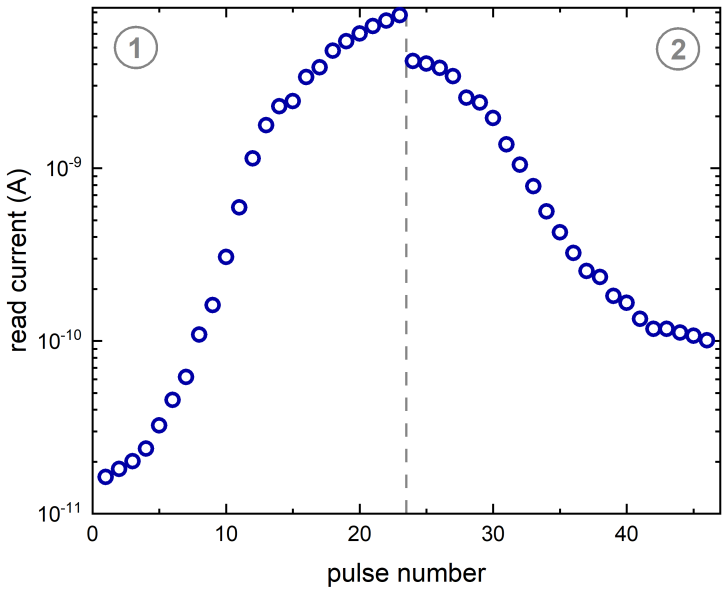

Figure 4.34.: A detailed measurement of the multilevel switching behaviour of the P(VDF-TrFE):PFO blend film device. In section (1) the amplitude of the voltage pulses was increased in 0.5 V steps from 21 V to 32 V and in section (2) it was decreased with the same step size between −21 V and −32 V.

ratio for pulsing was always below the one for sweeping for the same device (and both were measured with new devices, so that fatigue was not the reason for the difference). In the search for an explanation for this observation the results of the simulations for such a blend film device in [9] discussed in 2.4 were considered again. According to their study the charges transported through the semiconductor material in the accumulation channel at the interface are influenced by two processes. For one there is the charge injection at the interface of electrode/P(VDF-TrFE)/semiconductor dominated by tunnelling. The simulation shown in figure 2.6 (b) demonstrates that a calculation without the tunnelling contribution and therefore less charge injection would mean that both ON and OFF state levels are lowered. This does not match with the observation in 4.35.
On the other hand the calculation without the x-component of the polarisation in P(VDF-TrFE) (figure 2.6 (a)) has the effect that only the ON state current level is lowered and the ON/OFF ratio decreases. This is exactly the observation made for the pulsed addressing of the blend film device in figure 4.35. Hence the assumption is that pulsing compared to sweeping the voltage leads to a smaller x-polarisation component.
In the publication by Ghittorelli and Lenz [9]they only discuss the effect of a voltage

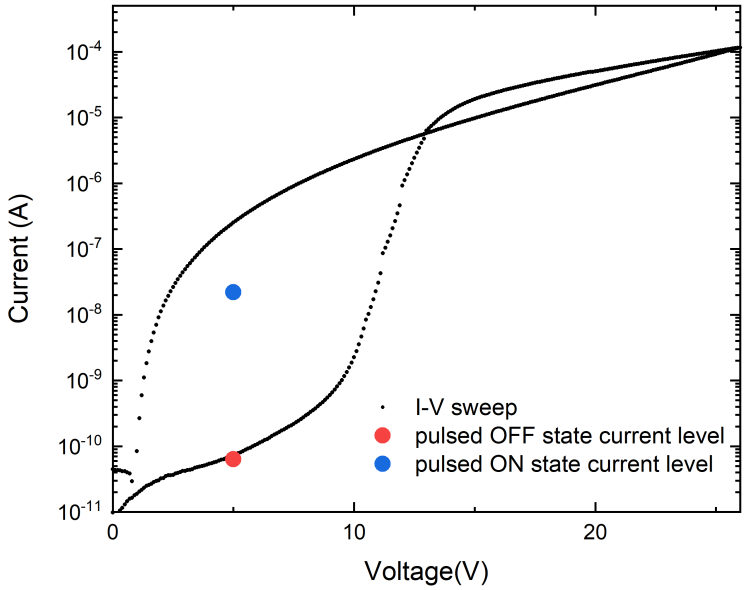

Figure 4.35.: Comparison of the ON and OFF state current levels reached with continuous application of increasing voltage and voltage pulses. For the swept measurement a higher ON state current can be reached.

sweep. They describe how the x-polarisation is induced by the charges at the ferroelectric/semiconductor interface influencing the dipole orientation in P(VDF-TrFE). It is also mentioned that a electric field in the opposite direction (like it is the case with the RESET pulses between two write pulses in the pulsed programming) leads to the charge carriers being pushed away from the interface and a pinch-off of the accumulation channel. In the supplementary note 6, which looks at the evolution of the interface accumulation layer, it is discussed, how the accumulation layer is build progressively during the slow sweep.
The assumption therefore is that during the pulsed measurement the x-polarisation in the ferroelectric is weaker, because the charges in the accumulation channel at the interface are only affecting the dipoles during the short duration of the pulses. Their simulations show a slow build-up of the charges and affecting the x-polarisation, so that the differences between the pulsing and sweeping of the voltage become important and have the effect observed in 4.35.

5. Conclusion

In this thesis new concepts for the fabrication and application of ferroelectric-semiconductor heterostructure devices were demonstrated.
An increase of the efficiency of a P(VDF-TrFE):semiconductor memory diode was achieved through an improvement in morphology of the device through development of a new processing method. This method uses porous P(VDF-TrFE) thin films with pores that continuously reach through the full height of the film. It also allows for the size and density of the pores to be adjusted through the processing parameters. The breath figure method under controlled humid atmosphere was used to create thin film with spherical pores, which were shaped into the desired columnar pore structure through a careful heating process under vacuum. It was shown that the density and average diameter of the pores increases with the humidity level during the spin-coating and the dependency on the heating time was analysed in detail.
The typical close-packed shallow pores on the surface, which are seen before heating, are flattened out in the initial minutes of heating and smaller, well distributed pores caused by water droplets, that had sunk down into the film are developed. These pores increase in diameter and density until after around 30 min the porous film is in the finished state with around 6% of the total area covered in pores and an average diameter of 400 nm (for a humidity of 80% during spin-coating).
These porous thin films (around 120 nm thickness) can be used for memory diodes by filling them with the semiconductor material. A device was produced through spin-coating the semiconducting polymer PFO onto the P(VDF-TrFE). After initial problems of filling the pores sufficiently without creating an high additional layer of PFO on the phase-separated film a well-behaved device was produced. Adjusting the spin-coating speed and heating the solution to 70 °C improved the backfilling. The device showed an efficiency, that was one order higher than a device produced by the common blend film method.
Apart from the P(VDF-TrFE):PFO memory diodes it was also attempted to create a lateral heterostructure by filling the porous P(VDF-TrFE) thin films with the small molecule TADF semiconductor 4CzIPN. This lead to dewetting problems, that could not be solved through various attempts with spin-coating and bar-coating techniques and surface treatment. More research has to be done to solve this problem.
This work also includes a study of the P(VDF-TrFE):PFO blend film device as a candidate for neuromorphic applications. Therefore detailed measurements using voltage pulses were conducted showing how the device can be brought into several stable intermediate states between the high resistance OFF state and the low resistance ON state by variation of the pulse width and amplitude. It could be seen that while the pulsed programming is reliable, the pulse read-out is problematic, since the measured

current values were dependent on read pulse duration and delay after the write pulse. A fast pulse train of reset, write and read pulses also had a strong fatigue effect on the device.
The retention time measurement showed very stable current levels, also for the multi-bit intermediate states, which is crucial for the information storage. The pulsing with repeated pulses of either pulse width or amplitude too small for an individual pulse to switch the polarisation state, proved not to be successful. The expected switching to the ON state with increasing number of pulses could not be observed. These measurements were also affected by the fatigue of the device through the fast pulsing. This could be improved in future measurements by changes in the materials used for the top electrode of the device.
It was possible to utilise the stable switching to intermediate polarisaton states to emulate synaptic behaviour. By applying two different pulse trains as the pre-spike and the post-spike pulse to both electrodes, it was possible to show spike timing dependent plasticity. The voltage amplitudes of the pre-spike pulses were chosen such that they were below the coercive field and would not change the polarisation state and only throught the simultaneous application of a post-pulse would the polarisation be chanced. The total difference of both pulses at the device was than large enough to cause either depression or potentiation of the resistance state emulating the changes in synaptic weight.
In a 2x2 memory array of P(VDF-TrFE):PFO blend film devices it was shown that all four devices could individually be programmed and read using a switching board to select each device. The devices in the array still suffered from crosstalk, so further improvements with a more advanced device structure have to be made.
The comparison of voltage sweeping and pulsing measurements showed a lower ON state current level reached for addressing the device with pulses. A possible explanation is that the pulsing leads to a lower x-polarisation in P(VDF-TrFE), which decreases the number of charges transported at the ferroelectric-semiconductor interface. A simulation could confirm this assumption.

A. Bibliography

[1] M. R. Niazi, R. Li, E. Q. Li, A. R. Kirmani, M. Abdelsamie, Q. Wang, W. Pan, M. M. Payne, J. E. Anthony, D.-M. Smilgies *et al.*, "Solution-printed organic semiconductor blends exhibiting transport properties on par with single crystals," *Nature communications*, vol. 6, no. 1, pp. 1–10, 2015.

[2] J. F. Scott and C. A. P. De Araujo, "Ferroelectric memories," *Science*, vol. 246, no. 4936, pp. 1400–1405, 1989.

[3] R. Naber, P. Blom, A. Marsman, and D. De Leeuw, "Low voltage switching of a spin cast ferroelectric polymer," *Applied Physics Letters*, vol. 85, no. 11, pp. 2032–2034, 2004.

[4] R. C. Naber, K. Asadi, P. W. Blom, D. M. de Leeuw, and B. de Boer, "Organic nonvolatile memory devices based on ferroelectricity," *Advanced materials*, vol. 22, no. 9, pp. 933–945, 2010.

[5] K. Asadi, M. Li, P. W. Blom, M. Kemerink, and D. M. de Leeuw, "Organic ferroelectric opto-electronic memories," *Materials Today*, vol. 14, no. 12, pp. 592–599, 2011.

[6] K. Asadi, M. Li, N. Stingelin, P. W. Blom, and D. M. de Leeuw, "Crossbar memory array of organic bistable rectifying diodes for nonvolatile data storage," *Applied Physics Letters*, vol. 97, no. 19, p. 242, 2010.

[7] K. Asadi, H. J. Wondergem, R. S. Moghaddam, C. R. McNeill, N. Stingelin, B. Noheda, P. W. Blom, and D. M. De Leeuw, "Spinodal decomposition of blends of semiconducting and ferroelectric polymers," *Advanced Functional Materials*, vol. 21, no. 10, pp. 1887–1894, 2011.

[8] J. J. Michels, A. J. Van Breemen, K. Usman, and G. H. Gelinck, "Liquid phase demixing in ferroelectric/semiconducting polymer blends: An experimental and theoretical study," *Journal of Polymer Science Part B: Polymer Physics*, vol. 49, no. 17, pp. 1255–1262, 2011.

[9] M. Ghittorelli, T. Lenz, H. S. Dehsari, D. Zhao, K. Asadi, P. W. Blom, Z. M. Kovács-Vajna, D. M. De Leeuw, and F. Torricelli, "Quantum tunnelling and charge accumulation in organic ferroelectric memory diodes," *Nature communications*, vol. 8, no. 1, pp. 1–8, 2017.

[10] K. Asadi, P. W. Blom, and D. M. De Leeuw, "The memoled: Active addressing with passive driving," *Advanced Materials*, vol. 23, no. 7, pp. 865–868, 2011.

[11] Z. Hu, M. Tian, B. Nysten, and A. M. Jonas, "Regular arrays of highly ordered ferroelectric polymer nanostructures for non-volatile low-voltage memories," *Nature materials*, vol. 8, no. 1, pp. 62–67, 2009.

[12] S. H. Sung and B. W. Boudouris, "Systematic control of the nanostructure of semiconducting-ferroelectric polymer composites in thin film memory devices," *ACS Macro Letters*, vol. 4, no. 3, pp. 293–297, 2015.

[13] T. Lenz, D. Zhao, G. Richardson, I. Katsouras, K. Asadi, G. Glaßer, S. T. Zimmermann, N. Stingelin, W. C. Roelofs, M. Kemerink *et al.*, "Microstructured organic ferroelectric thin film capacitors by solution micromolding," *physica status solidi (a)*, vol. 212, no. 10, pp. 2124–2132, 2015.

[14] K. Asadi, J. Wildeman, P. W. Blom, and D. M. de Leeuw, "Retention time and depolarization in organic nonvolatile memories based on ferroelectric semiconductor phase-separated blends," *IEEE transactions on electron devices*, vol. 57, no. 12, pp. 3466–3471, 2010.

[15] V. Khikhlovskyi, A. V. Gorbunov, A. J. van Breemen, R. A. Janssen, G. H. Gelinck, and M. Kemerink, "Multi-bit organic ferroelectric memory," *Organic electronics*, vol. 14, no. 12, pp. 3399–3405, 2013.

[16] Y. A. Genenko, S. Zhukov, S. V. Yampolskii, J. Schütrumpf, R. Dittmer, W. Jo, H. Kungl, M. J. Hoffmann, and H. von Seggern, "Universal polarization switching behavior of disordered ferroelectrics," *Advanced Functional Materials*, vol. 22, no. 10, pp. 2058–2066, 2012.

[17] D. Zhao, I. Katsouras, K. Asadi, W. A. Groen, P. W. Blom, and D. M. de Leeuw, "Retention of intermediate polarization states in ferroelectric materials enabling memories for multi-bit data storage," *Applied Physics Letters*, vol. 108, no. 23, p. 232907, 2016.

[18] Y. van De Burgt, A. Melianas, S. T. Keene, G. Malliaras, and A. Salleo, "Organic electronics for neuromorphic computing," *Nature Electronics*, vol. 1, no. 7, pp. 386–397, 2018.

[19] H. Li, R. Wang, S.-T. Han, and Y. Zhou, "Ferroelectric polymers for non-volatile memory devices: a review," *Polymer International*, 2020.

[20] A. K. Tagantsev, L. E. Cross, and J. Fousek, *Domains in ferroic crystals and thin films*. Springer, 2010, vol. 13.

[21] D. Zhao, I. Katsouras, K. Asadi, P. W. Blom, D. M. de Leeuw *et al.*, "Switching dynamics in ferroelectric p (vdf-trfe) thin films," *Physical Review B*, vol. 92, no. 21, p. 214115, 2015.

[22] R. J. Ouellette and J. D. Rawn, "1-structure and bonding in organic compounds," *Organic Chemistry. Boston: Elsevier*, pp. 1–39, 2014.

[23] J.-L. Brédas, D. Beljonne, V. Coropceanu, and J. Cornil, "Charge-transfer and energy-transfer processes in π-conjugated oligomers and polymers: a molecular picture," *Chemical reviews*, vol. 104, no. 11, pp. 4971–5004, 2004.

[24] H. Bässler and A. Köhler, "Charge transport in organic semiconductors," in *Unimolecular and supramolecular electronics I.* Springer, 2011, pp. 1–65.

[25] M. Gershenson, V. Podzorov, and A. Morpurgo, "Colloquium: Electronic transport in single-crystal organic transistors," *Reviews of modern physics*, vol. 78, no. 3, p. 973, 2006.

[26] S. Janietz, D. Bradley, M. Grell, C. Giebeler, M. Inbasekaran, and E. Woo, "Electrochemical determination of the ionization potential and electron affinity of poly (9, 9-dioctylfluorene)," *Applied physics letters*, vol. 73, no. 17, pp. 2453–2455, 1998.

[27] A. Monkman, C. Rothe, S. King, and F. Dias, "Polyfluorene photophysics," in *Polyfluorenes.* Springer, 2008, pp. 187–225.

[28] Y. Tao, K. Yuan, T. Chen, P. Xu, H. Li, R. Chen, C. Zheng, L. Zhang, and W. Huang, "Thermally activated delayed fluorescence materials towards the breakthrough of organoelectronics," *Advanced materials*, vol. 26, no. 47, pp. 7931–7958, 2014.

[29] C. Parker and C. Hatchard, "Triplet-singlet emission in fluid solutions. phosphorescence of eosin," *Transactions of the Faraday Society*, vol. 57, pp. 1894–1904, 1961.

[30] M. S. Park and J. K. Kim, "Breath figure patterns prepared by spin coating in a dry environment," *Langmuir*, vol. 20, no. 13, pp. 5347–5352, 2004.

[31] M. S. Park, W. Joo, and J. K. Kim, "Porous structures of polymer films prepared by spin coating with mixed solvents under humid condition," *Langmuir*, vol. 22, no. 10, pp. 4594–4598, 2006.

[32] D. Zhao, I. Katsouras, M. Li, K. Asadi, J. Tsurumi, G. Glasser, J. Takeya, P. W. Blom, and D. M. De Leeuw, "Polarization fatigue of organic ferroelectric capacitors," *Scientific reports*, vol. 4, p. 5075, 2014.

[33] D. S. Jeong, I. Kim, M. Ziegler, and H. Kohlstedt, "Towards artificial neurons and synapses: a materials point of view," *RSC advances*, vol. 3, no. 10, pp. 3169–3183, 2013.

[34] G.-q. Bi and M.-m. Poo, "Synaptic modifications in cultured hippocampal neurons: dependence on spike timing, synaptic strength, and postsynaptic cell type," *Journal of neuroscience*, vol. 18, no. 24, pp. 10 464–10 472, 1998.

[35] H.-J. Butt, B. Cappella, and M. Kappl, "Force measurements with the atomic force microscope: Technique, interpretation and applications," *Surface science reports*, vol. 59, no. 1-6, pp. 1–152, 2005.

[36] D. Kuzum, R. G. Jeyasingh, B. Lee, and H.-S. P. Wong, "Nanoelectronic programmable synapses based on phase change materials for brain-inspired computing," *Nano letters*, vol. 12, no. 5, pp. 2179–2186, 2012.

List of Figures

1.1. Comparison of phase separated ferroelectric-semiconductor heterostructures . . . 3

2.1. Polarisation in P(VDF-TrFE) . . . 5
2.2. Domain switching in P(VDF-TrFE) . . . 7
2.3. sp^2-hybridisation and double bonds in conjugated polymers . . . 8
2.4. Thermally activated delayed fluorescence . . . 9
2.5. Charge injection and accumulation in the heterostructure device . . . 11
2.6. Significance of tunneling and 2D polarisation for the performance of the blend film device . . . 12
2.7. Sketch of a typical breath figure pattern for water-miscible solvents . . . 13
2.8. Micrographs showing gold electrode delamination in fatigue measurements of P(VDF-TrFE) . . . 14
2.9. Synaptic potentiation and depression . . . 15

3.1. Chemical structure of **(a)** P(VDF-TrFE), **(b)** PFO and **(c)** 4CzIPN. . . 17
3.2. Illustration of the set-up used for controlling the conditions inside the spin-coater . . . 18
3.3. Switch board set-up for the 2x2 array . . . 22

4.1. Porous P(VDF-TrFE) film produced at 60% humidity . . . 25
4.2. Measurement of pore area and average pore diameter dependent on humidity level . . . 26
4.3. SEM images of porous P(VDF-TrFE) films with different heating times 27
4.4. Statistical analysis of porous P(VDF-TrFE) thin film heated for 30 minutes. . . . 28
4.5. AFM image of a porous P(VDF-TrFE) image for depth analysis . . . 29
4.6. Heating time dependency of the average diameter and density of pores in the P(VDF-TrFE) thin films. . . . 30
4.7. Sketch of the pore development with increasing heating time . . . 31
4.8. Current and photocurrent measured for the MEMOLED device using PFO as the semiconductor. . . . 34
4.9. Efficiency of the backfilled device in comparison with a common blend film device of P(VDF-TrFE) and PFO . . . 34
4.10. Images of devices backfilled with 4CzIPN as the semiconductor . . . 36
4.11. I-V measurement for several devices . . . 37
4.12. Exemplarily pulse train . . . 38
4.13. Pulsed read-out with Keithley 4200-SCS . . . 39

4.14. Charging during reset, write and read pulses 40
4.15. Multiple read-out pulses showing the on-going stabilisation of the polarisation state 40
4.16. Dependence of the read-out on write and read pulse width 41
4.17. Swept read-out after application of write pulses 42
4.18. Typical multilevel switching with pulsed addressing 43
4.19. Switching with pulses of increasing amplitude 44
4.20. Switching with pulses of increasing width 44
4.21. Switching to the ON and to the OFF state 45
4.22. Retention time measurement 46
4.23. Fatigue visible in the i-V sweep 47
4.24. Effect of fatigue on switching with increasing amplitude 47
4.25. Effect of fatigue on switching with increasing width 48
4.26. Repeated pulsing with low amplitude pulses 49
4.27. Repeated pulsing with longer pulse width 50
4.28. Repeated pulsing with higher amplitude 51
4.29. Repeated pulsing with high amplitude and shorter pulses 52
4.30. Switching with pre-spike and post-spike pulses 53
4.31. STDP simulation 54
4.32. Switching the polarisation state in a 2x2 array 55
4.33. Cross-talk in the 2x2 array 56
4.34. Detailed measurement of the multilevel switching behaviour 58
4.35. Comparison ON and OFF state current levels for swept and pulsed addressing 59

B. Appendix

B.1. Matlab code used for statistical analysis of four SEM images per sample

```
%first image
%select image
I=I1;
%defining scale bar
figure(1)
imshow(I)
h = imdistline(gca,[1250, 1125],[925,925]);
scale = 25000/getDistance(h);

%cropping image area
Ic = imcrop(I,[0 0 1300 1000]);
totalArea = (1300*scale)*(1000*scale);

%finding pores
[centersP, radiiP] = imfindcircles(Ic,[1 20],'ObjectPolarity'
    ,'dark');
viscircles(centersP, radiiP,'Color','b')
centers = centersP*scale;
radii= radiiP*scale;

%diameter, area, ratio
diameters = radii*2;
areas = radii.*radii * pi;

poreArea = sum(areas);
ratio = poreArea/totalArea;

%definitions
ratio1 = ratio;
diameters1 = diameters;

%second image
%select image
```

```
33 I=I2;
34 %defining scale bar
35 figure(2)
36 imshow(I)
37 h = imdistline(gca,[3002, 5020],[3600,3600]);
38 scale = 50000/getDistance(h);
39
40 %cropping image area
41 Ic = imcrop(I,[0 0 6100 3552]);
42 totalArea = (6100*scale)*(3552*scale);
43
44 %finding pores
45 [centersP, radiiP] = imfindcircles(Ic,[2 24],'ObjectPolarity'
       ,'bright');
46 viscircles(centersP, radiiP,'Color','b')
47 centers = centersP*scale;
48 radii= radiiP*scale;
49
50 %diameter, area, ratio
51 diameters = radii*2;
52 areas = radii.*radii * pi;
53
54 poreArea = sum(areas);
55 ratio = poreArea/totalArea;
56
57 %definitions
58 ratio2 = ratio;
59 diameters2 = diameters;
60
61 %third image
62 %select image
63 I=I3;
64 %defining scale bar
65 figure(3)
66 imshow(I)
67 h = imdistline(gca,[3002, 5020],[3600,3600]);
68 scale = 50000/getDistance(h);
69
70 %cropping image area
71 Ic = imcrop(I,[0 0 6100 3552]);
72 totalArea = (6100*scale)*(3552*scale);
73
74 %finding pores
75 [centersP, radiiP] = imfindcircles(Ic,[2 20],'ObjectPolarity'
```

```
    ,'bright');
viscircles(centersP, radiiP,'Color','b')
centers = centersP*scale;
radii= radiiP*scale;

%diameter, area, ratio
diameters = radii*2;
areas = radii.*radii * pi;

poreArea = sum(areas);
ratio = poreArea/totalArea;

%definitions
ratio3 = ratio;
diameters3 = diameters;

%fourth image
%select image
I=I4;
%defining scale bar
figure(4)
imshow(I)
h = imdistline(gca,[3002, 5020],[3600,3600]);
scale = 50000/getDistance(h);

%cropping image area
Ic = imcrop(I,[0 0 6100 3552]);
totalArea = (6100*scale)*(3552*scale);

%finding pores
[centersP, radiiP] = imfindcircles(Ic,[2 20],'ObjectPolarity'
    ,'bright');
viscircles(centersP, radiiP,'Color','b')
centers = centersP*scale;
radii= radiiP*scale;

%diameter, area, ratio
diameters = radii*2;
areas = radii.*radii * pi;

poreArea = sum(areas);
ratio = poreArea/totalArea;

%definitions
```

```
118 ratio4 = ratio;
119 diameters4 = diameters;
120
121 %statistical analysis
122 %average ratio
123 avRatio = (ratio1 + ratio2 + ratio3 + ratio4)/4;
124 diametersAll = [diameters1; diameters2; diameters3;
        diameters4];
125
126 %histogram
127 figure(5)
128 hist = histogram(diametersAll,'BinWidth',10)
129 xlabel('diameter(nm)');
130 ylabel('counts');
131
132 %fit
133 histfit(diametersAll,229,'normal')
134 Gaussian = fitdist(diametersAll,'normal')
```

B.2. Additional data and images on porous P(VDF-TrFE) films

heating time [min]	pore ratio [%]	average diameter [nm]
5	0.8	-
15	9.3	674 ± 12
30	5.6	621 ± 10
45	14.4	932 ± 14
60	17.6	923 ± 13

Table B.1.: Pore ratios and average pore diameters determined from statistical analysis of the SEM images of each sample spin-coated under ambient conditions and heated for different amounts of time in ambient condition in the oven. These measurements were conducted before the process was improved, so pore size were not very uniform, which made the analysis less accurate. The average diameter was calculated by fitting the normal distribution to the histogram of all diameters measured. For the sample heated for 5 min the dataset was to small to get a reliable fit.

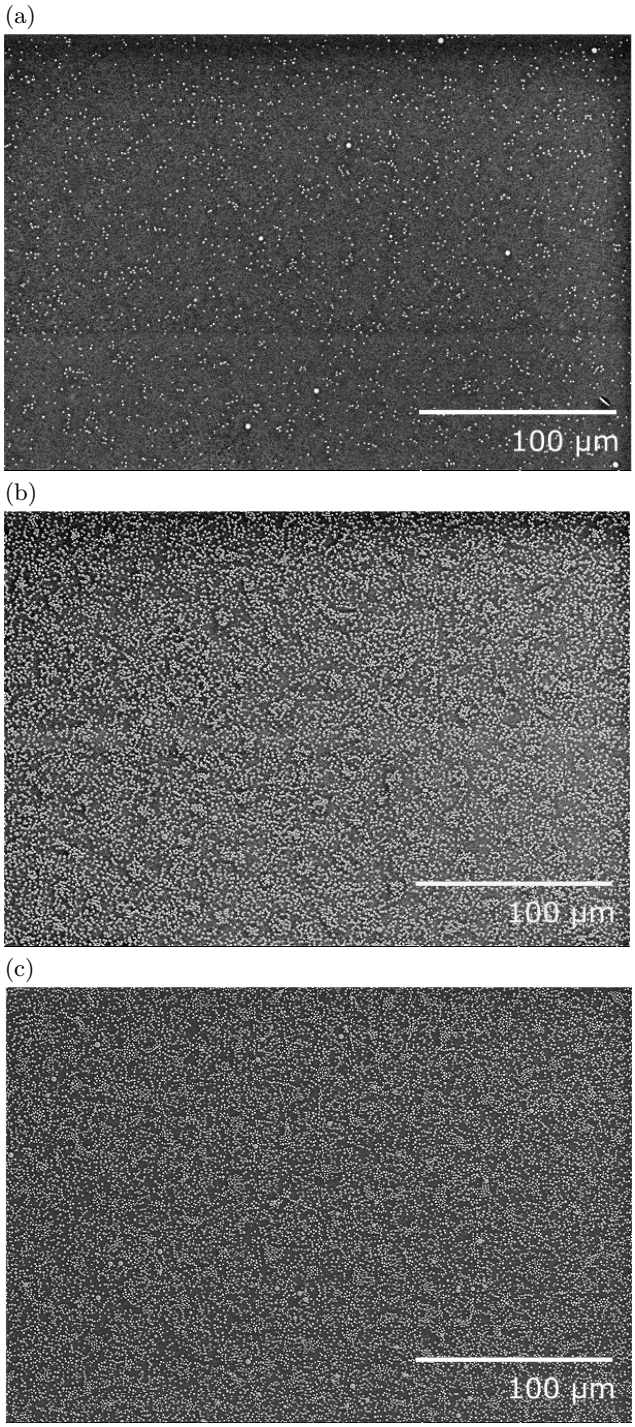

Figure B.1.: SEM images of measurement series with increasing humidity levels during the spin-coating of the porous P(VDF-TrFE) thin film, which were processed under not yet improved conditions.

humidity [%]	pore ratio [%]	average diameter [nm]
50	1.0	646 ± 8
60	5.2	756 ± 5
70	13.4	806 ± 9
80	17.6	793 ± 6

Table B.2.: Pore ratios and average pore diameters determined from statistical analysis of the SEM images of each sample with different humidity conditions during the spin-coating process. All samples were heated for 20 min. These measurements were conducted before the process was improved, so pores were not well distributed yet and formed clusters, which made the analysis less accurate. The average diameter was calculated by fitting the normal distribution to the histogram of all diameters measured.

(a)

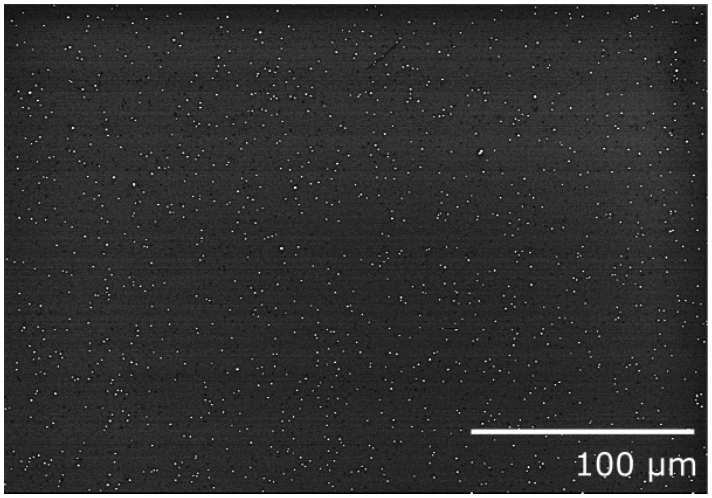

(b)

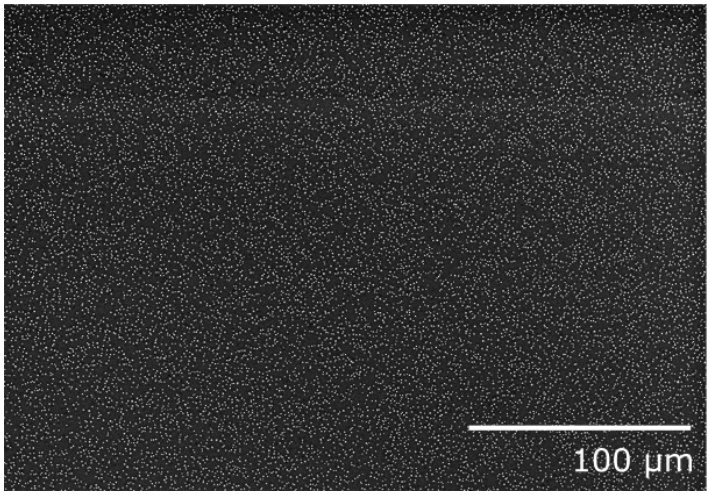

(c)

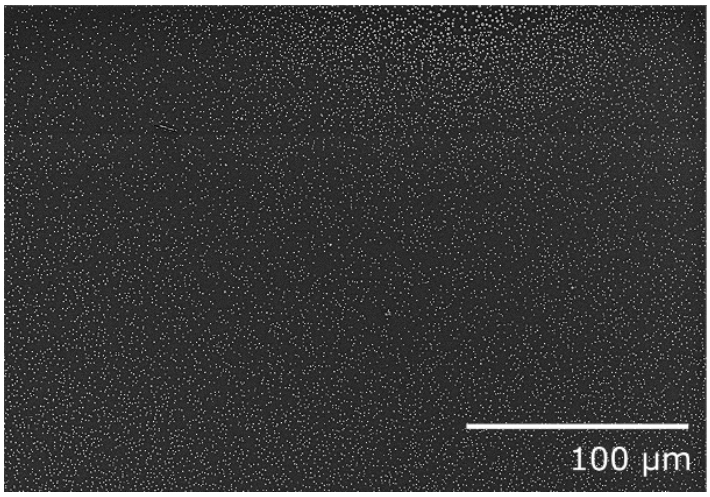

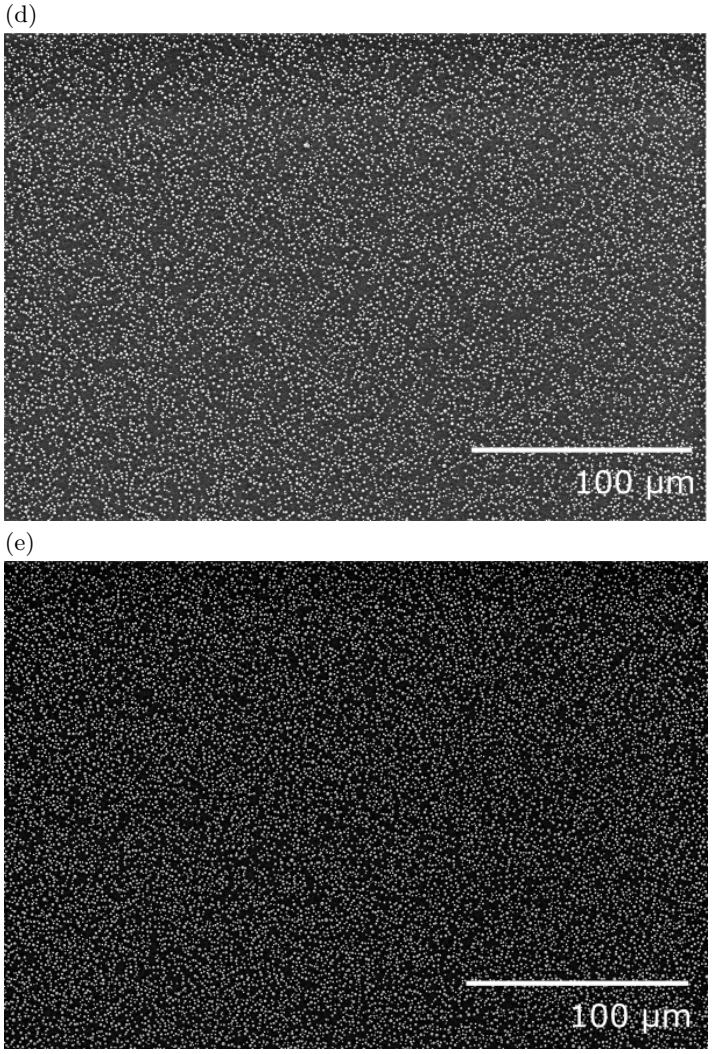

Figure B.2.: SEM images of initial measurement series with increasing heating time of the porous P(VDF-TrFE) thin film, which were processed under not yet improved conditions.

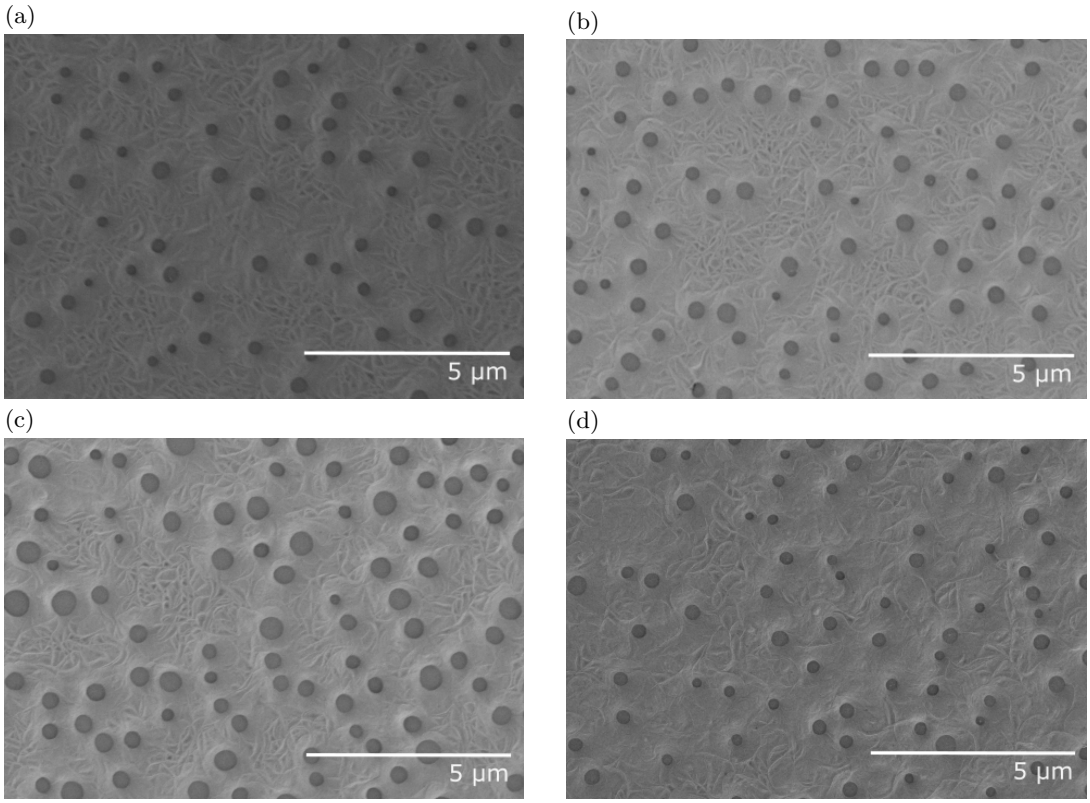

Figure B.3.: SEM images of porous P(VDF-TrFE) films with different heating times in the vacuum oven after the breath figure spin-coating of the solution. The samples shown here were heated for **(a)** 20 min, **(b)** 30 min, **(c)** 35 min and **(d)** 45 min.

B.3. Additional data on samples filled with 4CzIPN

	4CzIPN conc. in solution [wt%]	spin-coating speed [rpm]	comment	pore depth in 4CzIPN film [nm]	add layer thickness [nm]
1	1.0	1000	4CzIPN film not continuous	30 to 60	70 to 90
2	3.0	750	mostly continuous film, very rough surface	40 to 60	85 to 95
3	3.0	500	mostly continuous film, very rough surface	50 to 60	100 to 110
4	3.0	2000	4CzIPN film not continuous, just empty pores in the uncovered areas	-	20 to 30
5	3.0	3000	4CzIPN film not continuous, just empty pores in the uncovered areas	50 to 60	15 to 25
6	3.0	2000	4CzIPN film not continuous, surface treated with UV/ozone before spin-coating	40 to 60	30 to 35
7	3.0	2000	4CzIPN film looks continuous, treated with oxygen plasma (100W, 5s)	50 to 60	50 to 60
8	3.0	2000	4CzIPN film looks continuous, treated with nitrogen plasma (100W, 5s), rough surface	up to 120	no 4CzIPN deposited

Table B.3.: Overview of all the devices produced by spin-coating 4CzIPN onto the porous P(VDF-TrFE) thin films.

B.4. Additional data on film thickness in the array

device	thickness [nm]
A1	254.5 ± 7.4
A2	249.9 ± 3.9
A6	256.5 ± 5.9
A7	259.2 ± 12.0
A11	262.7 ± 6.3
A12	264.0 ± 8.8
A16	265.4 ± 4.9
A17	262.6 ± 1.0

Table B.4.: Thicknesses of the blend film for different devices used in the arrays in 4.2.7. The thickness was measured using a DEKTAK profilometer in four areas around each device and calculating the average. It can be observed that the devices used in the second array generally have a slightly higher thickness than those in the first array, but do not vary strongly from each other.

C. Acknowledgements

First of all I want to thank Dr. Kamal Asadi for allowing me to join MPIP and conduct my thesis on this very interesting topic. During the course of this year I have gained a lot of new knowledge and skills and I am grateful to you for giving me challenging tasks. Thank you for your support and guidance.
I want to especially thank Morteza Hassanpour for his help with the measurement focused part of my work and for many fruitful discussions. Thank you so much for always having an open door!
The whole AK Blom was very welcoming to me and always open to answer my questions. Special thanks to Paschalis Gkoupidenis for a very helpful contribution.
I want to thank Gunnar Glaßer for measuring SEM for me and Alfons Becker for support with the set-up of my measurements.
Special thanks also to Prof. Thomas Palberg for enabling me to take up this project outside of JGU.
I am thankful to my parents for enabling my studies and my sister for her support.